A recycling anti-transferrin receptor-1 monoclonal antibody as an efficient therapy for erythroleukemia through target up-regulation and antibody-dependent cytotoxic effector functions

Madeline Neiveyans, Rana Melhem, Christophe Arnoult, Thomas Bourquard, Marta Jarlier, Muriel Busson, Adrien Laroche, Martine Cerutti, Martine Pugnière, David Ternant, et al.

A recycling anti-transferrin receptor-1 monoclonal antibody as an efficient therapy for erythroleukemia through target up-regulation and antibody-dependent cytotoxic effector functions

[1,2]Madeline Neiveyans¶, [1,2]Rana Melhem¶, [3,4]Christophe Arnoult, [5]Thomas Bourquard, [2]Marta Jarlier, [1,2]Muriel Busson, [1,2]Adrien Laroche, [6]Martine Cerutti, [127]Martine Pugnière, [3,8]David Ternant [1,2]Nadège Gaborit, [1,2]Thierry Chardès, [5]Anne Poupon, ,[3,4]Valérie Gouilleux-Gruart, [1,2] Andre Pèlegrin, [1,2]Marie-Alix Poul

[1]IRCM, Institut de Recherche en Cancérologie de Montpellier; INSERM, U1194, Université de Montpellier, Montpellier, France

[2]Institut régional du Cancer de Montpellier, ICM, Montpellier, France

[3] CNRS UMR 7292 Génétique, Immunothérapie, Chimie et Cancer, Faculté de Médecine, CHRU de Tours

[4]Laboratoire d'Immunologie; Université François-Rabelais de Tours, Tours, France

[5] UMR INRA CNRS Physiologie de la reproduction et des comportements, Université de Tours, Nouzilly, France

[6] CNRS UPS3044 "Baculovirus et Thérapie" Saint-Christol-Lèz Alès, France

[7]PP2I, Plateforme Protéomique et Interactions Moléculaires, IRCM

[8]CHRU de Tours, Département de pharmacologie médicale, Tours, France

¶These authors have contributed equally to the work

*Corresponding author: Pr Marie-Alix Poul

Tel: +33 (0)467 61 24 04

Fax: +33 (0)467 61 37 87

Email: marie-alix.poul@inserm.fr

Running title: A recycling anti-TfR1 mAb for erythroleukemia treatment

Keywords: transferrin receptor 1, iron metabolism, leukemia, therapeutic antibody

Abbreviations

ADCC, Antibody-dependent cell-mediated cytotoxicity; CHO, Chinese hamster ovary; KO, knock-out; DFO, deferoxamine; *i.p.*, intraperitoneal *i.v.*; intravenous; mAb, monoclonal antibody; PBMC, peripheral blood mononuclear cells; PD, pharmacodynamics; PK, pharmacokinetics; *s.c.,* subcutaneous; TfR1 transferrin receptor 1; WT, wild type

Abstract:

Targeting transferrin receptor 1 (TfR1) with monoclonal antibodies is a promising therapeutic strategy in cancer as tumor cells often overexpress TfR1 and show increased iron needs. We have re-engineered six anti-human TfR1 single-chain variable fragment (scFv) antibodies into fully human $scFv_2$-Fcγ1 and IgG1 antibodies. We selected the more promising candidate (H7), based on its ability to inhibit TfR1-mediated iron-loaded transferrin internalization in Raji cells (B-cell lymphoma). The H7 antibody displayed nanomolar affinity for its target in both formats ($scFv_2$-Fcγ1 and IgG1), but cross-reacted with mouse TfR1 only in the $scFv_2$-Fc format. H7 reduced the intracellular labile iron pool and, contrary to what has been observed with previously described anti-TfR1 antibodies, upregulated TfR1 level in Raji cells. H7 $scFv_2$-Fc format elimination half-life was similar in FcRn knock-out and wild type mice, suggesting that TfR1 recycling contributes to prevent H7 elimination *in vivo*. *In vitro*, H7 inhibited the growth of erythroleukemia and B-cell lymphoma cell lines (IC_{50} 0.1 µg/mL) and induced their apoptosis. Moreover, the Im9 B-cell lymphoma cell line, which is resistant to apoptosis induced by rituximab (anti-CD20 antibody), was sensitive to H7. *In vivo*, tumor regression was observed in nude mice bearing ERY-1 erythroleukemia cell xenografts treated with H7 through a mechanism that involved iron deprivation and antibody-dependent cytotoxic effector functions. Therefore, targeting TfR1 using the fully human anti-TfR1 H7 is a promising tool for the treatment of leukemia and lymphoma.

Introduction

Iron deprivation is an emerging strategy in cancer therapeutics. Tumors have high iron content and rely on iron for their growth and progression.[1] Cancer stem cells also require iron for their survival.[2, 3] Iron levels in cells can be reduced with iron chelators,[4] which are already used in the clinic for iron overload disorders, or with monoclonal antibodies (mAbs) against transferrin receptor 1 (TfR1). TfR1 is the main receptor responsible for the cell iron supply through receptor-mediated internalization of serum Fe^{3+}-loaded transferrin (holo-Tf). Within the cell, Fe^{3+} is released, reduced, excluded from the early endosome by divalent metal ion transporter 1 (DMT1), and used for cell metabolism. Fe^{3+} excess is stored in ferritin, while TfR1 is recycled at the cell surface together with iron-free transferrin (apo-Tf).[5]

Several studies reported that *in vitro,* incubation of tumor cell lines with some anti-TfR1 mAbs decreases cell viability. The reasons for the decrease of cell viability (cell cycle arrest, mechanism of cell death, if observed) and its intensity largely vary depending on the cancer cell type (for example, hematopoietic cancer cells are more sensitive than solid cancer cells), on the TfR1 epitope recognized by the antibody, and on the antibody format (bivalency is generally required). Inhibition of cell viability is observed when anti-TfR1 mAbs reduce the cell iron supply through competition with holo-Tf,[5-8] or inhibition of TfR1 internalization,[9] or induction of TfR1 degradation.[10, 11]

We have recently obtained six rapidly internalized agonistic competitive anti-TfR1 single-chain variable-fragment (scFv) antibodies by phage display.[12] In this monovalent format, the F12 and H7 antibodies were the best holo-Tf competitors. *In vitro,* they

inhibited the growth of B-cell lymphoma and erythroleukemia cells (Raji and ERY-1 cell lines, respectively), and their efficiency increased upon conversion to the scFv homodimeric format ($scFv_2$). However, we found that in nude mice with established subcutaneous (*s.c.*) ERY-1 erythroleukemia cell xenografts, treatment with $scFv_2$-F12 significantly inhibited tumor growth, but tumor escape occurred.[6] We reasoned that because bivalent $scFv_2$ antibodies are prone to rapid elimination through the kidney due to their small size (50 kD)[13, 14] and because the Fc domain contributes to the long serum persistence of immunoglobulins *via* interaction with the neonatal Fc receptor (FcRn),[15] we might improve the *in vivo* therapeutic effect observed with the $scFv_2$ format by converting these anti-TfR scFv antibodies to formats containing a human Fcγ1 ($scFv_2$-Fc and full length IgG1, **Figure 1A**). These formats were chosen to improve the antibody pharmacokinetics (PK)[16] and to add effector functions (such as antibody-dependent cell-mediated cytotoxicity (ADCC) and phagocytosis (ADCP)),[17] to the scFv intrinsic inhibitory potential.

This report presents the *in vitro* characterization of the reformatted anti-TfR1 antibodies and their effects on hematological cancer cell lines, particularly of H7, the most efficient antibody that also displayed promising therapeutic efficacy *in vivo.*

Results

Antibody binding to TfR1 and inhibition of holo-Tf internalization

All the six parental anti-TfR1 scFv antibodies (H7, F12, C32, F2, H9, G9) could be converted into the $scFv_2$-Fc and IgG1 antibody formats **(Figure 1A),** with high production yields except for F12-IgG1. The initial characterization was done to verify that the new antibody formats could bind to TfR1 and inhibit TfR1-mediated holo-Tf

internalization, like the parental scFv antibodies.[6] The TfR1-expressing B-cell lymphoma Raji and mastocytoma P815 cell lines were used to test the binding to human and mouse TfR1, respectively (**Figure 1C**). Among the $scFv_2$-Fc antibodies, only H7, F12 and C32 also recognized mouse TfR1 **(Figure 1C, upper panel).** Among the IgG1 antibodies, H7 and C32 lost cross-reactivity to mouse TfR1 (**Figure 1C, lower panel**)**.** All six $scFv_2$-Fc antibodies inhibited internalization of 500 nM Alexa 488-conjugated holo-Tf (holo-Tf-A488), and H7-Fc was the most efficient with 70% inhibition at 5 µg/mL (50 nM) (**Figure 1D and S1**). Concerning the IgG1 antibodies, the inhibition of holo-Tf internalization by G9 and C32 was greatly reduced compared with the $scFv_2$-Fc format. H7-IgG1 was again the most efficient with 50% inhibition at 5 µg/mL (33 nM). Another anti-TfR1 mAb Ba120 (mouse IgG1), which shows inhibitory activity in leukemia models,[18] had no effect.

H7 was then chosen for more extensive characterization and comparison with Ba120. To test their capacity to block internalization of holo-Tf at physiological concentrations, 5 µg/mL of H7-Fc and H7-IgG1 (i.e., 50 nM and 33 nM, respectively) were mixed with 10 µM holo-Tf-A488. H7-Fc, but not H7-IgG1, still inhibited holo-Tf internalization in Raji cells (**Figure 2A, left panel and right panel, respectively**). Surprisingly, Ba120 increased holo-Tf internalization of more than 50%. The apparent affinity constant (EC_{50}) (**Figure 2B**) and the antibody concentration that blocked 50% of holo-Tf-A488 binding (used at 500 nM) to human TfR1 (IC_{50}) at 4°C in Raji cells (**Figure 2C**) were then determined. H7-Fc, H7-IgG1 and Ba120 displayed subnanomolar EC_{50} values, showing better binding to human TfR1 than holo-Tf (EC_{50} 16 nM) in the same conditions. Alternatively, H7-Fc and H7-IgG1 K_D (dissociation constant) values were also determined by surface plasmon resonance (SPR) using a steady-state fitting model

(Figure S2). Similar K_D (5 nM) were found for H7-Fc and H7-IgG1. Moreover, H7-Fc and H7-IgG1 fully inhibited holo-Tf binding to human TfR1 (IC_{50} of 5 nM), whereas Ba120 could only inhibit 50% of binding (**Figure 2C**), consistent with Ba120 inability to reduce holo-Tf internalization (**Figures 1D, 2A)**. When measured on mouse TfR1 using the p815 mouse cell line, H7-Fc displayed an EC_{50} of 0.8 nM **(Figure 2D),** in the same range as the EC_{50} for human TfR1 measured in Raji cells (0.3 nM). Finally, analysis of antibody (1 nM) binding in the presence of increasing concentrations of holo-Tf at 4°C showed that in Raji cells, H7-Fc binding to human TfR1 could be fully inhibited (IC_{50} 115 nM). Conversely, Ba120 binding was inhibited only by 50% even in the presence of a 1000 molar excess of holo-Tf (**Figure 2E**). Altogether, these results indicate a competitive inhibition of holo-Tf binding by H7 (*i.e.,* the H7 epitope on TfR1 overlaps with the holo-Tf binding site). Molecular modeling confirmed the TfR1-H7 (red) interaction, and showed that the Ba120 epitope (green) was away from the holo-Tf binding site (**Figure S3**).

Anti-TfR1 antibody intrinsic cytotoxic activity

After confirming that the ERY-1 and Raji cancer cell lines are sensitive to the iron chelator deferoxamine (DFO) (**Figure 3A**, **right panel**), these cell lines were used to test the effect of the H7 and Ba120 antibodies on cell growth. After 5 days of incubation, H7-Fc and H7-IgG1 strongly decreased the viability of both cell lines (IC_{50} in the range of 0.1 µg/mL) (**Figure 3A**). Conversely, Ba120 had a limited effect, in agreement with its lower competition with holo-Tf (**Figures 2C, 2E)**. Moreover, H7-IgG1 reduced rapidly (4h) the levels of the intracellular labile iron pool (LIP) in Raji and ERY-1 cells, while Ba120 had a more limited effect, especially at the lowest concentration used (1.5 µg/mL) (**Figure 3B**). In ERY-1 cells, apoptosis could be detected already after 1 day of incubation with

H7-Fc or H7-IgG1. After 3 days, the percentage of apoptotic cells was higher than 50% using 5nM of H7-Fc or H7-IgG1 (corresponding to 0.5 µg/mL and 0.75 µg/mL, respectively). Conversely, apoptosis was more limited with Ba120, even when used at high concentration (500 nM corresponding to 75 µg/mL) (**Figure 3C**). Apoptosis upon H7 treatment was also detected in Raji cells, with the same kinetics than in ERY-1 cells, but to a lesser extent, consistent with this cell line displaying autophagic, but not apoptotic cell death features upon iron deprivation. Then, to compare apoptosis induced by rituximab (anti-CD20 antibody) and by H7, the Bp3 and Im9 B-cell lymphoma cell lines (sensitive and resistant to rituximab-induced apoptosis, respectively) were incubated with H7 or rituximab. H7 strongly induced apoptosis in both cell lines, (**Figure 3D**). In Bp3 cells (rituximab-sensitive), the apoptotic rate was higher upon incubation with H7 than with rituximab (RX), although H7 effect was delayed compared with rituximab. Ba120 induced apoptosis in both cell lines, but was less efficient than H7 (**Figure 3D**). H7 also induced an early moderate free iron level decrease in both Bp3 and Im9 cell lines (**Figure S4**). Altogether, these *in vitro* data indicate that the holo-Tf uptake blockade by H7 induces apoptosis in leukemia and lymphoma cell lines, including those resistant to rituximab, likely by reducing the LIP.

H7 fate upon TfR1 binding

Upon binding of its natural ligand holo-Tf TfR1 is rapidly internalized and recycled after holo-Tf has released iron in the endosomes. In physiological conditions, TfR1 expression depends on LIP level through the regulation of TfR1 mRNA stability (for review, see Ref. 5). Previously described anti-TfR1 competitive inhibitory antibodies decreased TfR1 levels through antibody-dependent TfR1 routing to the lysosome where it is degraded. Degradation of TfR1 upon non-ligand competitive anti-TfR1 antibody has been shown to

be enhanced by high affinity or dimeric receptor binding compared to lower affinity or monomeric binding of TfR1.[19, 20] Here, incubation of Raji cells with the high affinity bivalent anti-TfR1 H7 (5 µg/mL) for 36h led to TfR1 level increase. Hypoxia-inducible factor 1-alpha (HIF-1α), the stability of which is affected by LIP through iron-dependent proteases,[21] was also strongly increased by H7 treatment **(Figure 3E)**. TfR1 increase upon treatment was strongly prevented by translation inhibition by cycloheximide and slightly increased by NH_4Cl treatment that limits lysosome acidification (Figure 3F). Conversely, holo-Tf and Ba120 treatment reduced TfR1 level after 36h of treatment (Figure 3E). These data suggest that unlike Ba120, H7 does not interfere with TfR1 recycling and induces limited TfR1 degradation. Finally, H7 binding to TfR1 was not decreased at pH 6 compared with pH 7 (**Figure S5**), indicating that, like apo-Tf, H7 might not be released in the endosome and could be mostly recycled back to the cell surface together with TfR1. However, unlike apo-Tf, which has reduced affinity for TfR1 at extracellular pH,[22] H7 should not dissociate at the cell surface, and, therefore, reduce strongly the accessibility of the recycled TfR1 to iron-charged holo-Tf, thus explaining H7 high iron deprivation efficiency.

To explore the potential consequences of the TfR1 modulation by H7 observed *in vitro* on H7 PK/pharmacodynamics (PD), the biodistribution of a mixture of ^{125}I-labeled H7-Fc and ^{131}I-labeled irrelevant $scFv_2$-Fc antibodies was evaluated in mice. The $scFv_2$-Fc format was chosen because, differently from the IgG1 format, it can cross-react with mouse TfR1 (**Figure 1C**). Nude mice bearing subcutaneous ERY-1 tumor cell xenografts received one intravenous (*i.v.)* injection of the two antibody mixture (6 µg, 5 µCi/each) (n=4). The percentage of the injected dose (%ID) after 48 h in each individual mouse was similar for H7-Fc and the irrelevant $scFv_2$-Fc antibody, consistent with the well-

described enhanced permeability and retention (EPR) effect in tumors[23] (**Figure 4A, left panel**). Individual variations among animals could be explained by the different tumor sizes (300 to 800 mm^3). However, as indicated by the organ repartition index, H7-Fc specificity for mouse TfR1 resulted in increased radioactivity associated with the tumor compared with the irrelevant $scFv_2$-Fc antibody (ratio >1) (**Figure 4A, right panel, and Figure S6).** In a parallel experiment, H7-Fc (80 µg) was *i.v.* injected in C57Bl/6 wild type (WT) mice or in C57Bl/6 FcRn knock-out (KO) mice and titered by ELISA in the serum (**Figure 4B)**. As seen **Figure 4B,** in WT mice, H7-Fc was cleared from the serum more rapidly than the irrelevant $scFv_2$-Fc, likely due to its binding to mouse TfR1. AUC and serum clearance (CL) classic constants are reported in Table S1. A two-compartment model (plasma and intracellular/central compartments) was designed to describe the cellular uptake and cellular recycling of the antibodies (see materials and methods section and **Figure 4C**). This model is derived from previously published models.[24, 25] In our model, the apparent distribution volume (V_D) was higher for H7-Fc than for Irr-$scFv_2$-Fc, both in WT and C57Bl/6 FcRnKO mice, consistent with higher intracellular localization of H7-Fc (2.5 mL versus 1 mL for H7-Fc and Irr-$scFv_2$-Fc, respectively, (LRT, $p<0.0005$)). As expected,[26] the recycling of Irr-$scFv_2$-Fc (k_{CS}) was decreased in FcRnKO mice due to the lack of lysosomal rescue associated to the absence of FcRn[15] and consistently, its elimination half-life $T_{1/2}$ was lower in FcRnKO compared to WT background (1.7 to 7.9 days, LRT, $p<0.0005$). However, strikingly, if the recycling of H7-Fc was also decreased in FcRnKO mice, its elimination half-life was not affected and remained around 4 to 5 days in both genetic backgrounds (**Figure 4D and Table I**). Since both FcRn and antibody factors were quantified simultaneously in the multivariate model, the effects due to FcRn or TfR1 binding and recycling are measured independently. Therefore, this could indicate that H7-Fc is protected from elimination

by its binding to TfR1. Altogether, the biodistribution and PK results reveals a dominant target mediated stabilization mechanism for H7-Fc.

Finally, nude mice with established *s.c.* ERY-1 tumor cell xenografts were treated with H7-Fc (5 mg/kg via intraperitoneal (*i.p.*) administration twice a week) or phosphate-buffered saline (PBS) (n=5 animals/group). After 4 weeks of treatment, two animals were cured in the H7-Fc group. Moreover, western blot analysis of the tumors **(Figure 4E)** showed that TfR1 levels were increased in the tumors of the other three mice treated with H7-Fc compared with the tumors of the PBS group. IHC analysis of one tumor for each group (900 mm^3) with an anti-TfR1 antibody showed higher TfR1 staining in the H7-Fc treated sample (**Figure 4F**). These data indicate that H7-Fc treatment upregulates TfR1 *in vivo*, as observed *in vitro*, suggesting that tumors treated with H7 undergo iron deprivation.

The H7 antibody can mediate ADCC

Cytotoxic effector cells require interaction with the Fc portion of an antibody to initiate FcγR-dependent degranulation and perform ADCC. TfR1 is a rapidly internalizing receptor, and H7 was isolated on the basis of its rapid internalization.[27] To determine whether this feature affected H7-mediated ADCC, the antibody was added to the target cells (Raji cells or HMC11 cells) for 30 min, to allow TfR1 internalization, before addition of freshly prepared peripheral blood mononuclear cells (PBMC) for 3h. In this assay, H7-IgG1, induced ADCC in HMC11 cells ($TfR1^{pos}$, $CD117^{pos}$, $CD20^{neg}$) and Raji cells ($TfR1^{pos}$, $CD117^{neg}$, $CD20^{pos}$), with comparable efficiency **(Figure 5A),** while the anti-CD117 mAb 2D1 (human IgG1), and the anti-CD20 rituximab (human IgG1) mediated toxicity only on HMC11 and Raji cells, respectively**.** Compared with H7-IgG1, H7-Fc effect was more

limited and observable only after 16h of incubation with PBMC **(Figure 5B).** This difference was confirmed in two other cell lines (**Figure S7**).

In vivo effects of H7

Nude mice with established *s.c.* ERY-1 tumors were treated with PBS (controls) or H7-Fc (100 µg per *i.p.* injection twice a week) for 4 weeks (n=7/group). Mice were sacrificed when tumors reached 1600 mm^3. Compared with controls, tumor growth in the H7-Fc group was significantly reduced ($p<0.05$) during the treatment time. Specifically, three mice responded to the treatment, and one was totally cured (**Figure 6 A-B**). However, survival was not significantly improved (**Figure 6C**). Weight loss was not observed in any mouse during the experiment. In the next experiment, (**Figure 6 D**), in which H7-IgG1 (200 µg per *i.p.* injection twice a week) was used instead of H7-Fc, tumor regression was observed in all mice treated with H7-IgG1, but in none of the PBS group or of the irrelevant IgG1 group (n=6 mice/group). In five mice of the H7-IgG1 group, tumors were undetectable at day 60 after the end of the treatment. Finally, treatment with a non-glycosylated variant of H7-IgG1 (H7-IgG1 del297, defective in ADCC and ADCP due to reduced affinity for the Fcγ receptors and defective in complement-dependent cytotoxicity, due to reduced affinity for C1q,[28] (n=6 mice) inhibited tumor growth ($p<0.05$) and two mice were cured. Therefore, H7 treatment reduced ERY-1 tumor growth, with a stronger effect observed with the IgG1 than the $scFv_2$-Fc format. Altogether, these results indicate that the higher therapeutic efficiency of H7-IgG1 compared with H7-Fc correlates with its higher ADCC activity *in vitro.*

Discussion

Starting from a panel of anti-TfR1 scFv antibodies that were isolated for their rapid cell internalization upon antigen binding, we engineered bivalent antibodies harboring a human Fcγ1. We found that for the $scFv_2$-Fcγ1 format, H7-Fc was the most efficient antibody concerning inhibition of holo-Tf uptake (**Figure 1D**). This was due to H7 great efficiency in blocking holo-Tf binding (2 log lower molar concentrations of H7 are required to block holo-Tf binding, and 2 log higher molar concentrations of holo-Tf are required to block H7 binding) (**Figure 2 C, E**). H7-IgG1 maintained this feature, but lost cross-reactivity to mouse TfR1 (**Figures 1C, 2D**). This loss of cross-reactivity after reformatting has previously been observed with other antibodies.[29, 30] Despite the similar apparent affinity of the two H7 formats measured in Raji cells or by SPR on recombinant human TfR1 (**Figure 2B, S2**), H7-IgG1-mediated ADCC in Raji cells was strong, whereas H7-Fc mediated limited ADCC (**Figure 5**). This is surprising because several studies reported that the Fc domain of $scFv_2$-Fc antibodies can direct effector cell toxicity to antigen-expressing target cells.[31, 32] However, geometry differences in the $scFv_2$-Fc and the IgG1 formats that modify Fc region access to the FcyR of immune effector cells and affect antibody-dependent cell-mediated killing have also been recently reported.[33] As the two formats were not produced using the same cell system, this discrepancy could be also due to differences in glycosylation enzymes between HEK-293 T (production of H7-Fc) and Chinese hamster ovary (CHO) cells (production of H7-IgG1). Indeed, in HEK-293 T cells, the increased content of N-acetylneuraminic acid (sialic acid) of N-glycostructures[34] can reduce the affinity for FcγRIIIa, the receptor on natural killer cells.[35, 36]

Incubation of cells with H7-Fc or H7-IgG1 increased TfR1 levels (Figure 3E) similarly to incubation with the 50 kD dimeric $(scFv)_2$ H7 antibody (H7-$scFv_2$).[6] Therefore, the presence of an Fc region did not change the receptor modulation. To our knowledge, this property is unique because, like the anti-TfR1 Ba120 mAb tested in this study, [18] other previously described high affinity anti-TfR1 antibodies in the IgG1 format decrease TfR1 level through traffic diversion and degradation within lysosomes.[10, 11] TfR1 normal trafficking is not extensively diverted to lysosome by H7 binding **(Figure 3F).** Combined with the efficient iron deprivation that promotes TfR1 translation, this property contributes to the TfR1 level increase observed *in vitro* and *in vivo* upon H7 treatment (**Figures 3E, 4D**). H7-mediated iron deprivation is higher than with Ba120 in ERY-1 and Raji cells lines (**Figure 3B**). We also find that Ba120 increases rapidly soluble iron levels in Bp3 and Im9 cells lines (**Figure S4**). Because Ba120 induces TfR1 degradation, visible after 36h in Raji cells (**Figure 3E**), the increase in soluble iron level mediated by Ba120 is probably only transient. As H7 binds with similar affinity to TfR1 at extracellular and endosomal pH (**Figure S5B**), H7 may be recycled at the cell surface with the receptor after it has induced its internalization, thus immediately preventing TfR1 association with extracellular holo-Tf. This mechanism of action could contribute to the fast and strong effect observed upon incubation with H7 *in vitro* (apoptosis detected after 36h in the 4 cell lines tested (**Figure 3 C-D**)). The increased efficiency (>2 log) of ERY-1 cell viability inhibition by the bivalent H7-IgG1 (IC_{50} 0.5 nM), H7-Fc (IC_{50} 1.4 nM) and H7-$scFv_2$ (IC_{50} 2 nM)[6] compared with the monovalent H7-scFv (IC_{50} 200 nM)[6] suggests that these bivalent antibodies can bind to two proximal TfR1 receptors on cells in which the receptor is present at high density. Accordingly, lower toxicity is expected in cells that express low levels of TfR1, as previously suggested for the anti-TfR1 mAb A24[7] and demonstrated for the anti-TfR1 JST-TFR09 antibody.[8] In agreement, no obvious toxicity

was observed in mice treated with H7-Fc (cross-reactive with mouse TfR1) for 1 month compared with untreated mice (PBS), indicating that despite background TfR1 expression in many tissues, iron deprivation due to H7 should have limited toxicity *in vivo*. However, since non-competitive effector competent anti-TfR1 antibodies have been shown to transiently elicit acute clinical signs and to clear immature blood reticulocytes in mice,[37] it is not excluded that such a toxicity may occur with the competitive anti-TfR1 H7 of this study. This will need to be determined using an effector function competent variant of $scFv_2$-Fc H7 in mice.

As TfR1 is expressed at low level by many cell types, we hypothesized that antigen-dependent recycling of H7 could protect this antibody from degradation in an FcRn-like process. Indeed, FcRn and TfR1 share similar intracellular trafficking and both can rescue their respective ligands from lysosomal degradation.[15, 38-40] To test this hypothesis, because human Fcγ1 binding to mouse FcRn receptors allows relevant PK observations in mice,[41] we compared the PK of the cross-reactive H7-Fc in WT and FcRnKO mice. In our model, compared to WT mice, the elimination half-life of H7-Fc was only weakly affected in FcRnKO mice (**Figure 4D**), while the elimination half-life of the irrelevant $scFv_2$-Fc antibody was dramatically reduced, as previously reported for this antibody format.[32, 42] Moreover, the apparent volume of distribution of H7-Fc was more than twice larger compared to the apparent volume of distribution of the irrelevant $scFv_2$-Fc. Additionally, H7 bound with similar affinity to TfR1 at extracellular and endosomal pH. These observations are consistent with the hypothesis of a mechanism of stabilization of H7 through TfR1 binding and recycling. This could also explain the antitumor effect of H7 in a $scFv_2$ format in nude mice harboring *s.c.* ERY-1 tumors, although no therapeutic effect was expected because of its small size (50 kDa) and potential fast serum clearance through kidneys.[43, 44] H7 specificity and its unique mode

of interaction with TfR1 (it acts like an exact mimic of the natural ligand) could increase its persistence *in vivo* through an FcRn-like mechanism that is independent of the Fc part of the antibody.

In vitro, H7 had a strong inhibitory effect in different lymphoma and leukemia cell lines, including the rituximab-resistant B-cell lymphoma cell line Im9 (**Figure 3 A,D**). H7 drastically reduced cell viability of Raji and ERY-1 cells (IC_{50} in the range of 0.1 µg/mL) and induced apoptosis in ERY-1, Raji, Bp3 and Im9 cells. In Raji cells, in addition to limited apoptosis, autophagic cell death features were observed with increased cell granularity and volume (not shown), as previously described with H7-$scFv_2$.[6] Ba120 showed a delayed and weaker effect compared with H7. *In vitro,* IC_{50} as low as those for H7 in cancer cells have been observed only with the recently described anti-TfR1 JST-TFR09 antibody in adult T-cell leukemia/lymphoma (ATLL) cells. [8] Moreover, in Raji and ERY-1 cells, H7 also induced immunogenic cell death features[45] with exposure of calreticulin at the cell surface of pre-apoptotic cells and ATP release (data not shown). Similar effects were also observed upon incubation with DFO in both cell lines (data not shown). Therefore, in addition to the direct effect on tumor cells and on the recruitment of cytotoxic cells, H7-mediated iron deprivation could also prime the adaptive immune response.

In vivo, in nude mice xenografted with ERY-1 erythroleukemia cells, H7-IgG1 treatment allowed curing five of the six mice with established tumors. Iron deprivation is part of the mechanism of action of H7-IgG1 because H7-Fc and H7-IgG1 del297 (both with limited effector function) reduced tumor growth compared with PBS or irrelevant antibody treatment. However, effector functions improve the effect of TfR1 targeting

because H7-IgG1 was clearly more efficient than H7-Fc and H7-IgG1 del297. The upregulation of TfR1 mediated by LIP decrease through the Iron regulatory protein/iron responsive element (IRP/IRE) system,[1] likely potentiates antibody-mediated immune effector recruitment to tumor cells in H7-IgG1-treated mice, and, therefore, iron deprivation may both participate directly and indirectly to the overall drastic efficiency of H7-IgG1 treatment. The lower H7-Fc efficacy could also be linked to a lower localization in the tumor compared with H7-IgG1 because of antigen-driven localization of the cross-reactive H7-Fc in other tissues. It could be interesting to produce an effector function-competent H7-Fc in CHO cells and test its effect in this erythroleukemia model, or in syngeneic tumor models to address H7 therapeutic effect and toxicity in a more relevant setting.

In conclusion, we developed a promising fully human anti-TfR1 antibody with unique PK/PD properties that displays high therapeutic efficiency in an erythroleukemia mouse model with no apparent toxicity. As TfR1 expression is increased in many tumors, this antibody could also be active in other cancer types.

Material and methods

Antibodies, cells and reagents

The $scFv_2$-Fc antibodies were produced in HEK-293 T cells[46] and the H7-IgG1 in CHO cells (EVITRIA, Switzerland). The anti-TfR1 H7-IgG1 del297 and Ba120 mAbs were provided by A. Fontayne (LFB, France). The Bp3, Im9,[47] Raji, and ERY-1[48] cell lines were grown in RPMI; the P815 and HMC11 cell lines in IMDM (both media were supplemented with 10% fetal bovine serum and antibiotics). Commercial antibodies and

reagents for fluorescent-activated cell sorting (FACS), western blotting and immunohistochemistry (IHC) are listed in the on-line supplement.

In vitro assays

Holo-Tf uptake, apparent affinity and ligand competition, cell viability and apoptosis assays were performed as described. Intracellular free iron levels were measured using calcein, as described in Ref. 49. For the ADCC assay, target cells were stained with the PKH26 fluorescent dye. Then, 50 µL of stained cells (50,000 cells) were combined with 50 µL of antibody for 30 minutes, followed by 50 µL (2.5 10^6 cells) of PBMC at 37°C for 3h. Cells were stained with 7-AAD before FACS analysis. Details are given in the on-line supplement. Cells were incubated with 50 µg/mL cycloheximide and 10 mM NH_4Cl (SIGMA) in some experiments.

Pharmacokinetics

Ten WT C57Bl/6 (Janvier, Saint-Berthevin, France) and FcRnKO (B6.Cg-Fcgrt^{tm1Dcr})[50] (Jackson Laboratory, Bar Harbor, ME) mice received an *i.v.* retro-orbital injection of 80 µg of $scFv_2$-Fc (single dose). From 2h to day 21 post-injection, blood samples were collected and $scFv_2$-Fc titered by ELISA (see on-line supplement). A two-compartment model was designed to describe cellular uptake of antibodies. Compartments were serum (S) and intracellular (C) and k_{SC}, k_{CS} and k_E are cellular uptake, cellular recycling and intracellular elimination rate constants, respectively (**Figure 4C**). The PK of antibodies was analyzed using population PK modelling using Monolix®2018 suite (Lixoft, Orsay, France). Interindividual and residual variabilities of the PK parameters were estimated using exponential and proportional models, respectively. The association of FcRn (WT vs. KO) and antibody (Irrelevant $scFv_2$-Fc vs H7-Fc) factors was

tested as dichotomous covariates on PK parameter interindividual distributions. These covariates were tested using likelihood ratio tests (LRT) based on objective function value (OFV). From pairs of nested models (i.e., models with vs. without covariate), the difference between their OFV was tested using a chi-square test. A covariate was considered as significant if corresponding p-value was < 0.05.

Biodistribution

A mixture of ^{125}I-labeled H7-Fc and ^{131}I-labeled irrelevant scFv$_2$-Fc (6 µg, 5 µCi each) was injected (*i.v.)* in four 6 to 8-week-old female athymic mice (Harlan Labs) xenografted with ERY-1 cells (2 × 10^6) by *s.c*. injection in the flank and in four 6 to 8-week-old BALB/C mice (Envigo, France). After 48h, mice were killed and the radioactivity of both iodine isotopes was quantified in all organs and tissues by using a dual-channel γ scintillation counter.

In vivo erythroleukemia model and H7-based therapy

When tumors reached an average volume of 100 mm^3, mice bearing *s.c.* ERY-1 tumors were randomized in different treatment groups (6 to 8 animals/group): 100 µg of H7-Fc, 200 µg of H7-IgG1, H7-IgG1 del297 or PBS, all by *i.p.* injection twice a week for 4 weeks. For survival analysis, mice were sacrificed when tumors reached a volume of 1,600 mm^3. Mice were considered as cured when tumor was non more palpable. The statistical analyses are described in the on-line supplement.

References

1. Torti SV, Torti FM. Iron and cancer: more ore to be mined. Nat Rev Cancer 2013; 13:342-55.

2. Basuli D, Tesfay L, Deng Z, Paul B, Yamamoto Y, Ning G, et al. Iron addiction: a novel therapeutic target in ovarian cancer. Oncogene 2017; 36:4089-99.
3. Rychtarcikova Z, Lettlova S, Tomkova V, Korenkova V, Langerova L, Simonova E, et al. Tumor-initiating cells of breast and prostate origin show alterations in the expression of genes related to iron metabolism. Oncotarget 2017; 8:6376-98.
4. Heath JL, Weiss JM, Lavau CP, Wechsler DS. Iron deprivation in cancer--potential therapeutic implications. Nutrients 2013; 5:2836-59.
5. Daniels TR, Delgado T, Rodriguez JA, Helguera G, Penichet ML. The transferrin receptor part I: Biology and targeting with cytotoxic antibodies for the treatment of cancer. Clin Immunol 2006; 121:144-58.
6. Crepin R, Goenaga AL, Jullienne B, Bougherara H, Legay C, Benihoud K, et al. Development of human single-chain antibodies to the transferrin receptor that effectively antagonize the growth of leukemias and lymphomas. Cancer research 2010; 70:5497-506.
7. Moura IC, Lepelletier Y, Arnulf B, England P, Baude C, Beaumont C, et al. A neutralizing monoclonal antibody (mAb A24) directed against the transferrin receptor induces apoptosis of tumor T lymphocytes from ATL patients. Blood 2004; 103:1838-45.
8. Shimosaki S, Nakahata S, Ichikawa T, Kitanaka A, Kameda T, Hidaka T, et al. Development of a complete human IgG monoclonal antibody to transferrin receptor 1 targeted for adult T-cell leukemia/lymphoma. Biochemical and biophysical research communications 2017; 485:144-51.
9. Lesley JF, Schulte RJ. Inhibition of cell growth by monoclonal anti-transferrin receptor antibodies. Mol Cell Biol 1985; 5:1814-21.
10. Lepelletier Y, Camara-Clayette V, Jin H, Hermant A, Coulon S, Dussiot M, et al. Prevention of mantle lymphoma tumor establishment by routing transferrin receptor toward lysosomal compartments. Cancer research 2007; 67:1145-54.
11. Ng PP, Helguera G, Daniels TR, Lomas SZ, Rodriguez JA, Schiller G, et al. Molecular events contributing to cell death in malignant human hematopoietic cells elicited by an IgG3-avidin fusion protein targeting the transferrin receptor. Blood 2006; 108:2745-54.
12. Goenaga AL, Zhou Y, Legay C, Bougherara H, Huang L, Liu B, et al. Identification and characterization of tumor antigens by using antibody phage display and intrabody strategies. Molecular immunology 2007; 44:3777-88.
13. Bayliss LE, Kerridge PM, Russell DS. The excretion of protein by the mammalian kidney. J Physiol 1933; 77:386-98.
14. Wu AM. Engineered antibodies for molecular imaging of cancer. Methods 2014; 65:139-47.
15. Ghetie V, Ward ES. FcRn: the MHC class I-related receptor that is more than an IgG transporter. Immunology today 1997; 18:592-8.
16. Zuckier LS, Chang CJ, Scharff MD, Morrison SL. Chimeric human-mouse IgG antibodies with shuffled constant region exons demonstrate that multiple domains contribute to in vivo half-life. Cancer research 1998; 58:3905-8.
17. Bruhns P, Jonsson F. Mouse and human FcR effector functions. Immunological reviews 2015; 268:25-51.
18. Loisel S, Andre PA, Golay J, Buchegger F, Kadouche J, Cerutti M, et al. Antitumour effects of single or combined monoclonal antibodies directed against membrane antigens expressed by human B cells leukaemia. Molecular cancer 2011; 10:42.
19. Yu YJ, Zhang Y, Kenrick M, Hoyte K, Luk W, Lu Y, et al. Boosting brain uptake of a therapeutic antibody by reducing its affinity for a transcytosis target. Sci Transl Med 2011; 3:84ra44.

20. Bien-Ly N, Yu YJ, Bumbaca D, Elstrott J, Boswell CA, Zhang Y, et al. Transferrin receptor (TfR) trafficking determines brain uptake of TfR antibody affinity variants. The Journal of experimental medicine 2014; 211:233-44.
21. Bruick RK, McKnight SL. Transcription. Oxygen sensing gets a second wind. Science 2002; 295:807-8.
22. MacGillivray RT, Moore SA, Chen J, Anderson BF, Baker H, Luo Y, et al. Two high-resolution crystal structures of the recombinant N-lobe of human transferrin reveal a structural change implicated in iron release. Biochemistry 1998; 37:7919-28.
23. Matsumura Y, Maeda H. A new concept for macromolecular therapeutics in cancer chemotherapy: mechanism of tumoritropic accumulation of proteins and the antitumor agent smancs. Cancer research 1986; 46:6387-92.
24. Hansen RJ, Balthasar JP. Effects of intravenous immunoglobulin on platelet count and antiplatelet antibody disposition in a rat model of immune thrombocytopenia. Blood 2002; 100:2087-93.
25. Guilleminault L, Maillet A, S. Pesnel, Paintaud G, Congy-Jolivet N, G. Thibault G, et al. Aerosoltherapy in lung cancer. European Respiratory Society 2008; Abstract 1547.
26. Chen N, Wang W, Fauty S, Fang Y, Hamuro L, Hussain A, et al. The effect of the neonatal Fc receptor on human IgG biodistribution in mice. mAbs 2014; 6:502-8.
27. Poul MA, Becerril B, Nielsen UB, Morisson P, Marks JD. Selection of tumor-specific internalizing human antibodies from phage libraries. J Mol Biol 2000; 301:1149-61.
28. Tao MH, Morrison SL. Studies of aglycosylated chimeric mouse-human IgG. Role of carbohydrate in the structure and effector functions mediated by the human IgG constant region. J Immunol 1989; 143:2595-601.
29. Krebs B, Rauchenberger R, Reiffert S, Rothe C, Tesar M, Thomassen E, et al. High-throughput generation and engineering of recombinant human antibodies. Journal of immunological methods 2001; 254:67-84.
30. Thie H, Toleikis L, Li J, von Wasielewski R, Bastert G, Schirrmann T, et al. Rise and fall of an anti-MUC1 specific antibody. PloS one 2011; 6:e15921.
31. De Lorenzo C, Tedesco A, Terrazzano G, Cozzolino R, Laccetti P, Piccoli R, et al. A human, compact, fully functional anti-ErbB2 antibody as a novel antitumour agent. Br J Cancer 2004; 91:1200-4.
32. Powers DB, Amersdorfer P, Poul M, Nielsen UB, Shalaby MR, Adams GP, et al. Expression of single-chain Fv-Fc fusions in Pichia pastoris. Journal of immunological methods 2001; 251:123-35.
33. Weber F, Bohrmann B, Niewoehner J, Fischer JAA, Rueger P, Tiefenthaler G, et al. Brain Shuttle Antibody for Alzheimer's Disease with Attenuated Peripheral Effector Function due to an Inverted Binding Mode. Cell Rep 2018; 22:149-62.
34. Croset A, Delafosse L, Gaudry JP, Arod C, Glez L, Losberger C, et al. Differences in the glycosylation of recombinant proteins expressed in HEK and CHO cells. J Biotechnol 2012; 161:336-48.
35. Scallon BJ, Tam SH, McCarthy SG, Cai AN, Raju TS. Higher levels of sialylated Fc glycans in immunoglobulin G molecules can adversely impact functionality. Molecular immunology 2007; 44:1524-34.
36. Cymer F, Beck H, Rohde A, Reusch D. Therapeutic monoclonal antibody N-glycosylation - Structure, function and therapeutic potential. Biologicals 2017.
37. Couch JA, Yu YJ, Zhang Y, Tarrant JM, Fuji RN, Meilandt WJ, et al. Addressing safety liabilities of TfR bispecific antibodies that cross the blood-brain barrier. Sci Transl Med 2013; 5:183ra57, 1-12.

38. Goebl NA, Babbey CM, Datta-Mannan A, Witcher DR, Wroblewski VJ, Dunn KW. Neonatal Fc receptor mediates internalization of Fc in transfected human endothelial cells. Mol Biol Cell 2008; 19:5490-505.
39. Ramalingam TS, Detmer SA, Martin WL, Bjorkman PJ. IgG transcytosis and recycling by FcRn expressed in MDCK cells reveals ligand-induced redistribution. EMBO J 2002; 21:590-601.
40. Tuma P, Hubbard AL. Transcytosis: crossing cellular barriers. Physiological reviews 2003; 83:871-932.
41. Ober RJ, Radu CG, Ghetie V, Ward ES. Differences in promiscuity for antibody-FcRn interactions across species: implications for therapeutic antibodies. Int Immunol 2001; 13:1551-9.
42. Kenanova V, Olafsen T, Crow DM, Sundaresan G, Subbarayan M, Carter NH, et al. Tailoring the pharmacokinetics and positron emission tomography imaging properties of anti-carcinoembryonic antigen single-chain Fv-Fc antibody fragments. Cancer research 2005; 65:622-31.
43. Demignot S, Pimm MV, Baldwin RW. Comparison of biodistribution of 791T/36 monoclonal antibody and its Fab/c fragment in BALB/c mice and nude mice bearing human tumor xenografts. Cancer research 1990; 50:2936-42.
44. Holliger P, Hudson PJ. Engineered antibody fragments and the rise of single domains. Nature biotechnology 2005; 23:1126-36.
45. Hernandez C, Huebener P, Schwabe RF. Damage-associated molecular patterns in cancer: a double-edged sword. Oncogene 2016; 35:5931-41.
46. Le Gall M, Crepin R, Neiveyans M, Auclair C, Fan Y, Zhou Y, et al. Neutralization of KIT Oncogenic Signaling in Leukemia with Antibodies Targeting KIT Membrane Proximal Domain 5. Molecular cancer therapeutics 2015; 14:2595-605.
47. Brien G, Trescol-Biemont MC, Bonnefoy-Berard N. Downregulation of Bfl-1 protein expression sensitizes malignant B cells to apoptosis. Oncogene 2007; 26:5828-32.
48. Ribadeau Dumas A, Hamouda NB, Leriche L, Piffaut MC, Bonnemye P, Kuen RL, et al. Establishment and characterization of a new human erythroleukemic cell line, ERY-1. Leuk Res 2004; 28:1329-39.
49. Roth M, Will B, Simkin G, Narayanagari S, Barreyro L, Bartholdy B, et al. Eltrombopag inhibits the proliferation of leukemia cells via reduction of intracellular iron and induction of differentiation. Blood 2012; 120:386-94.
50. Arnoult C, Brachet G, Cadena Castaneda D, Azzopardi N, Passot C, Desvignes C, et al. Crucial Role for Immune Complexes but Not FcRn in Immunization against Anti-TNF-alpha Antibodies after a Single Injection in Mice. J Immunol 2017; 199:418-24.

Disclosure of Potential Conflicts of Interest

No potential conflicts of interest were disclosed.

Acknowledgments

The authors thank Alexandre Fontayne (LFB) for the production of the IgG1 formats of the antibodies.

Grant Support

This work was supported by the program "Investissement d'avenir" grant agreement: Labex MabImprove, ANR-10-LABX-53-01. RM was partly supported by a PhD fellowship from the Lebanese University and AISOS, AL was supported by a PhD fellowship from the Labex MabImprove.

Legends to the figures

Figure 1: Preliminary characterization of the reformatted anti-TfR1 scFvs

(A) Graphic representation of the $scFv_2$-Fc and the IgG1 formats, in grey variable domains (light grey, VH; dark grey, VL), in black, constant domains. **(B)** Validation of TfR1 surface expression on the lymphoma Raji cell line (human) and P815 mastocytoma cells (mouse) by FACS (FC500 cytometer) with a commercial mouse anti-human TfR1 IgG or a rat anti-mouse TfR1 IgG (10 µg/mL) followed by anti-mouse IgG or anti-rat IgG fluorescent secondary antibodies, respectively, or with fluorescent holo-Tf (500 nM) **(C)** Detection of the binding of the panel of anti-TfR1 antibodies reformatted into bivalent scFv by fusion to Fc (upper panel) or in full-length human IgG1 (lower panel) to the Raji or the mouse P815 cell lines, as indicated. Binding is detected with an anti-human IgG1 antibody conjugated to FITC and FACS analysis (FC500 cytometer). Dark grey peaks represent fluorescent background of the secondary antibody alone or, in case of the detection of fluorescent holo-Tf binding, cell autofluorescence. **(D)** $scFv_2$-Fc (left panel) and full length IgG1 (right panel) interference with fluorescent holo-Tf internalization in Raji cells: antibodies at the indicated concentrations are combined with fluorescent holo-Tf (500 nM) and incubated at 37°C with Raji cells for 3 h then cells are collected, washed with PBS and analyzed by FACS. Results are expressed in Mean Fluorescent Intensity (MFI) relative to cells incubated with fluorescent holo-Tf only. Irr, irrelevant antibody of the same format. The data shown are representative of 3 independent experiments.

Figure 2: Characterization of the anti-TfR1 H7 scFv$_2$-Fc and full length IgG1 antibodies

(A) Interference of H7-Fc and H7-IgG1 (5 µg/mL) (left and right panel, respectively) with the internalization of 10 µM or 1 µM Alexa 488-conjugated holo-Tf, measured as in **Figure 1**. **(B)** Apparent affinity of H7-Fc, H7-IgG1 and Ba120 (mouse monoclonal anti-TfR1 IgG1) and of Alexa 488-conjugated holo-Tf for human TfR1 measured by detection of the binding of increasing concentrations of antibody/holo-Tf in Raji cells at 4°C. Bound antibodies were detected with a mouse anti-human-Fc fluorescent antibody and analyzed by FACS (Gallios cytometer); results are expressed as MFI in function of the primary antibody concentration. The EC_{50} values (nM) are indicated. **(C)** Measurement of the fluorescence signal in Raji cells after incubation (at 4°C for 1h) with 500 nM Alexa 488-conjugated holo-Tf and increasing concentrations of H7-Fc, H7-IgG1, irrelevant scFv$_2$-Fc antibody, or Ba120. Results are expressed as the % MFI compared with cells incubated with holo-Tf alone. **(D)** Apparent affinity of H7-Fc and H7-IgG1 for mouse TfR1 measured by detection of the binding of increasing concentrations of antibody in P815 cells at 4°C as in B, **(E)** H7-Fc (left panel) and Ba120 (right panel) binding to TfR1 in Raji cells in the presence of increasing concentrations of holo-Tf. Bound antibodies were detected by FACS with anti-human-Fc or anti-mouse-Fc fluorescent secondary antibodies, (Gallios cytometer) and results expressed as MFI. The IC_{50} values (nM) are indicated. In B, D and E, similar EC_{50} and IC_{50} determinations were obtained in 2 to 3 independent experiments in the same setting.

Figure 3: Functional properties of the anti-TfR1 H7 scFv$_2$-Fc and full length IgG1 antibodies

(A) Viability of ERY-1 erythroleukemia (upper panel) and Raji B-cell lymphoma (lower panel) cells was assessed with the MTS assay after incubation with H7-Fc, H7-IgG1 or Ba120 (5 days). Results are expressed as the percentage of viable cells compared with untreated cells. The iron chelator DFO was also tested in the same conditions; the IC_{50} values (µg/mL for antibodies or µM for DFO) are indicated. The irrelevant $scFv_2$-Fc antibody (Irr-Fc) did not have any effect on cell viability (H7-Fc panel). **(B)** Variation of intracellular soluble iron levels in ERY-1 and Raji cells induced by incubation with DFO, H7-IgG1 or Ba120 at 37°C for 4h and 8h. Before addition of the antibodies, cells were labeled with the intracellular iron-chelating dye calcein. Calcein fluorescence, which is quenched when chelated to iron, was measured by FACS. Results are expressed as the percentage of change in the fluorescence signal relative to untreated cells (NT). Apoptosis induction in **(C)** ERY-1 and Raji cells and in **(D)** Bp3 and Im9 B-cell lymphoma cells after incubation with H7-Fc, H7-IgG1 (or an irrelevant antibody in the same format, Irr.), Ba120, or rituximab (RX, human IgG1; only in D) for the indicated time. After treatment, cells were collected and stained with Annexin conjugated to FITC and 7-AAD, and analyzed by FACS. Results are expressed as the percentage of Annexin+/7AAD- cells (i.e., early apoptotic cells) compared with untreated cells. (E) Comparative effect of TfR1 H7-IgG1 (5 µg/mL) and holo-Tf (10 µM) treatment (36 h) of Raji cells on TfR1 and HIF-1α levels. Cells were alternatively treated with Ba120 or the corresponding irrelevant antibody format at the same concentration. After treatment, protein extracts (20 µg) separated by SDS-PAGE (7% polyacrylamide separation gel) and analyzed by Western Blot. Quantification relative to actin is represented under the Western Blot. The data shown are representative of 3 independent experiments. Irr, irrelevant. In **(F),** Raji cells were treated as in E. for 18 hr in the presence of 10 mM NH_4Cl or 50 µg/mL cycloheximide (CHX) as indicated or not, and TfR1 levels were quantifyed like in E.

Figure 4: PK/PD of the crossreactive anti-TfR1 H7 scFv$_2$-Fc format (H7-Fc)

(A) Four nude mice bearing ERY-1 tumors were injected *i.v.* with a mixture of ^{125}I-labelled H7-Fc and ^{131}I irrelevant scFv$_2$-Fc (6 µg, 5 µCi each). After 48 h, mice were killed and the radioactivity in all organs and tissues was quantified by dual-channel γ scintillation counting of both iodine isotopes. Results are expressed as the % of the injected dose (ID) in the whole mice (left panels) or as the organ specificity index at the time of sacrifice (^{125}I % cpm relative to total body dose)/(^{131}I % cpm relative to total body dose for a specific organ) (right panels; raw data are available in **Fig. S6.)** (**B**) Two groups of 10 WT and FcRnKO C57Bl/6 mice were injected *i.v.* with 4 mg/kg of H7-Fc (about 80 µg) (left panel) or irrelevant scFv$_2$-Fc (right panel). Antibody concentration in serum at various time after injection was evaluated by ELISA by Fc domain detection and normalized for each mice to the concentration measured 2 h. after injection. **(C)** Two-compartment model describing antibody PK, where k_{SC}, k_{CS} and k_E are cellular uptake, cellular recycling and intracellular elimination rate constants, respectively (see methods for details). **(D)** Apparent volume of distribution (V_D), serum elimination half-life ($T_{1/2}$) and recycling constant k_{CS} and determined by the model, ***, p<0,005 **(E, F)** Groups of 5 nude mice with ERY-1 subcutaneous tumors of 200 mm3 were treated for 4 weeks with either PBS or H7-Fc (5 mg/kg injected *i.p.* 2 times a week) and **(E)** all tumors were then processed for protein extraction and Western Blot for TfR1 detection, the relative intensity of the TfR1 band and the size of individual tumors at the time of analysis are indicated. **(F)** One tumor of similar size at the time of sacrifice in each group (900 mm^3) was analyzed by IHC for TfR1 expression.

Figure 5: ADCC on Raji cells using the anti-TfR1 H7 scFv$_2$-Fc and full length IgG1 antibodies

Live lymphoma Raji cells **(A, B)** or mastocytoma leukemic HMC11 cells **(A)** were stained with the fluorescent dye PKH-67 and then pre-incubated with H7-IgG1 (**A,B**), H7-Fc (**B**), anti-CD117 (2D1) or anti-CD20 (RX) human IgG1 at the indicated concentrations for 30 min before addition of freshly prepared PBMC (effector cells/target cells ratio = 50). After 3h (or 16h), cells were collected and stained with the 7-AAD fluorescent dye. The percentage of dead cells (7AAD$^+$) among the target PKH-67$^+$ cells was determined by FACS analysis. In **A**, experiments were in duplicate.

Figure 6: Therapeutic effect of the anti-TfR1 H7 scFv$_2$-Fc and full length IgG1 antibodies

ERY-1 cells were implanted *s.c*. into nude mice. When tumors reached 200 mm^3, (**A, B, C**) H7-Fc (100µg in 200 µL of PBS) or PBS (200 µL) or (**D, E, F**) H7-IgG1, unglycosylated H7-IgG1 (H7-IgG1 del297) or irrelevant IgG1 (200µg in 200 µL PBS), or PBS (200 µL), were injected *i.p* twice a week for 4 weeks and tumor growth was monitored. **(A, D)** Tumor volume of individual mice or **(B, E)** average tumor volumes and **(C, F)** percent of mice with tumor volume<1600 mm^3 are represented as a function of time. Shaded zone represent treatment period. Experiments A,B,C and D,E,F were performed independently. *, $p<0.05$, **, $p<0.01$

Figure 1

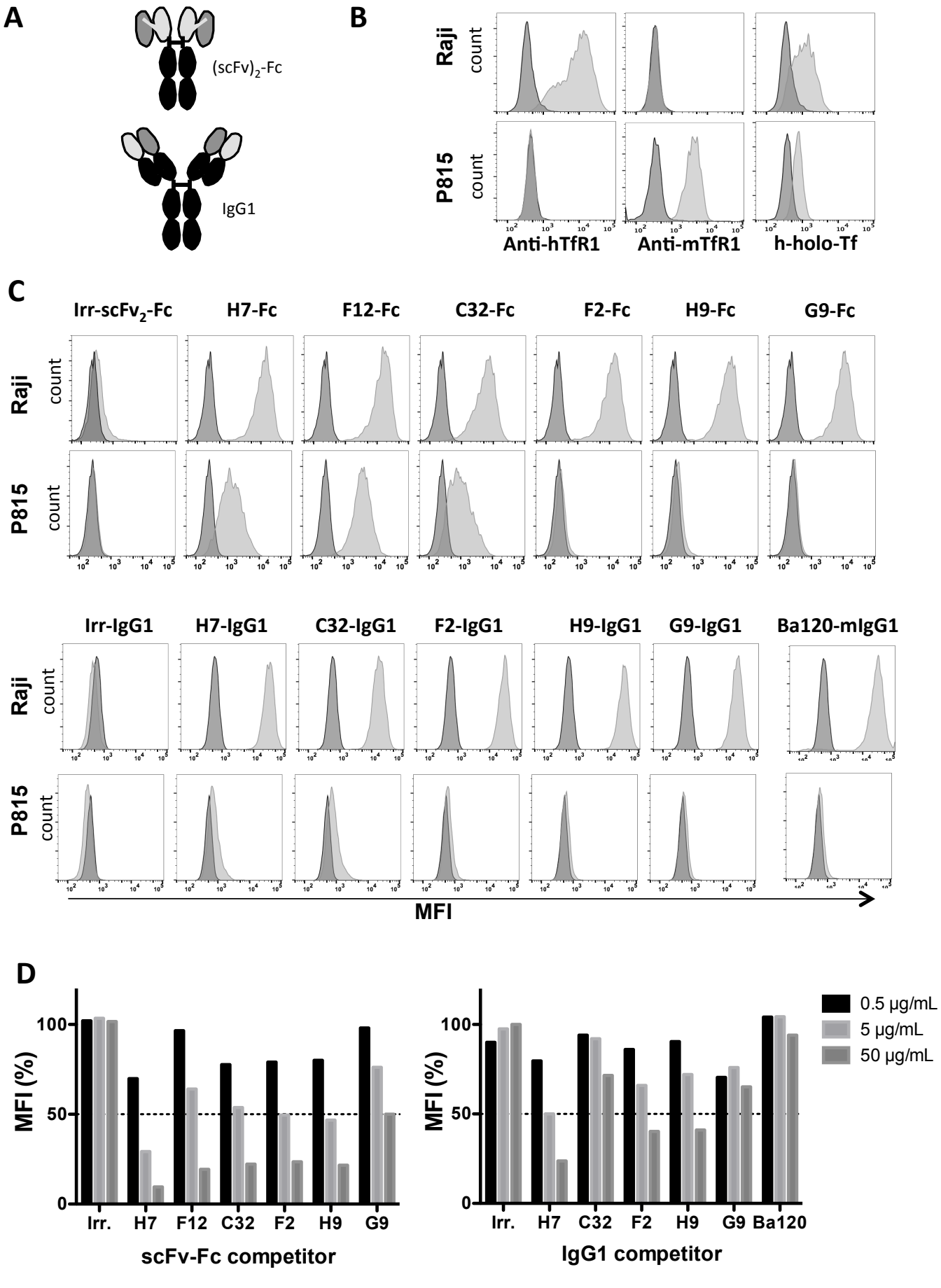
A
(scFv)2-Fc
IgG1
B
Raji
P815
count
Anti-hTfR1
Anti-mTfR1
h-holo-Tf
C
Irr-scFv2-Fc
H7-Fc
F12-Fc
C32-Fc
F2-Fc
H9-Fc
G9-Fc
Irr-IgG1
H7-IgG1
C32-IgG1
F2-IgG1
H9-IgG1
G9-IgG1
Ba120-mIgG1
MFI
D
MFI (%)
100
50
0
Irr.
H7
F12
C32
F2
H9
G9
scFv-Fc competitor
Ba120
IgG1 competitor
0.5 µg/mL
5 µg/mL
50 µg/mL

Figure 2

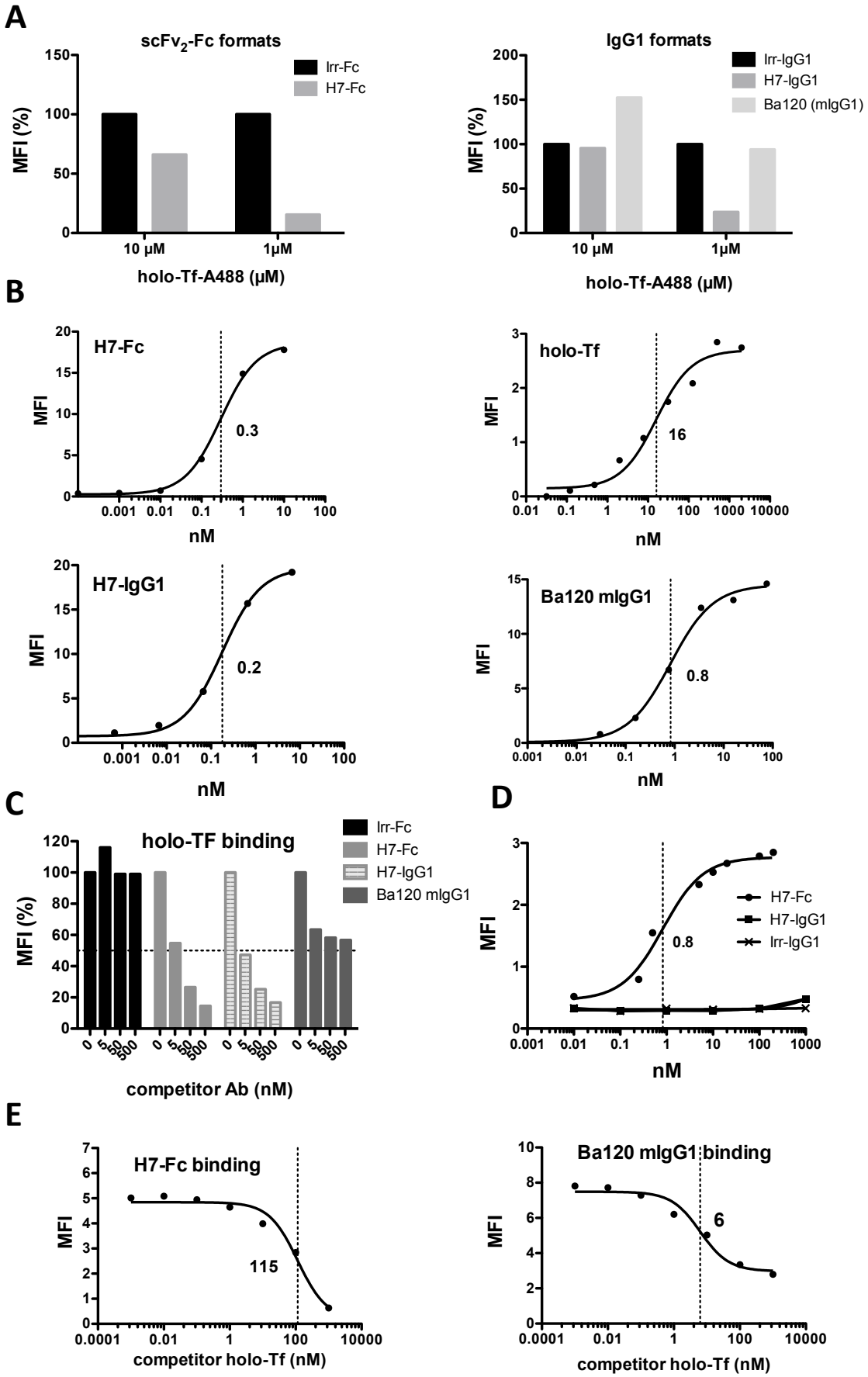
A
scFv2-Fc formats
Irr-Fc
H7-Fc
MFI (%)
10 µM
1µM
holo-Tf-A488 (µM)
IgG1 formats
Irr-IgG1
H7-IgG1
Ba120 (mIgG1)
B
H7-Fc
0.3
holo-Tf
16
H7-IgG1
0.2
Ba120 mIgG1
0.8
MFI
nM
C
holo-TF binding
competitor Ab (nM)
D
H7-Fc
H7-IgG1
Irr-IgG1
E
H7-Fc binding
115
Ba120 mIgG1 binding
6
competitor holo-Tf (nM)

Figure 3

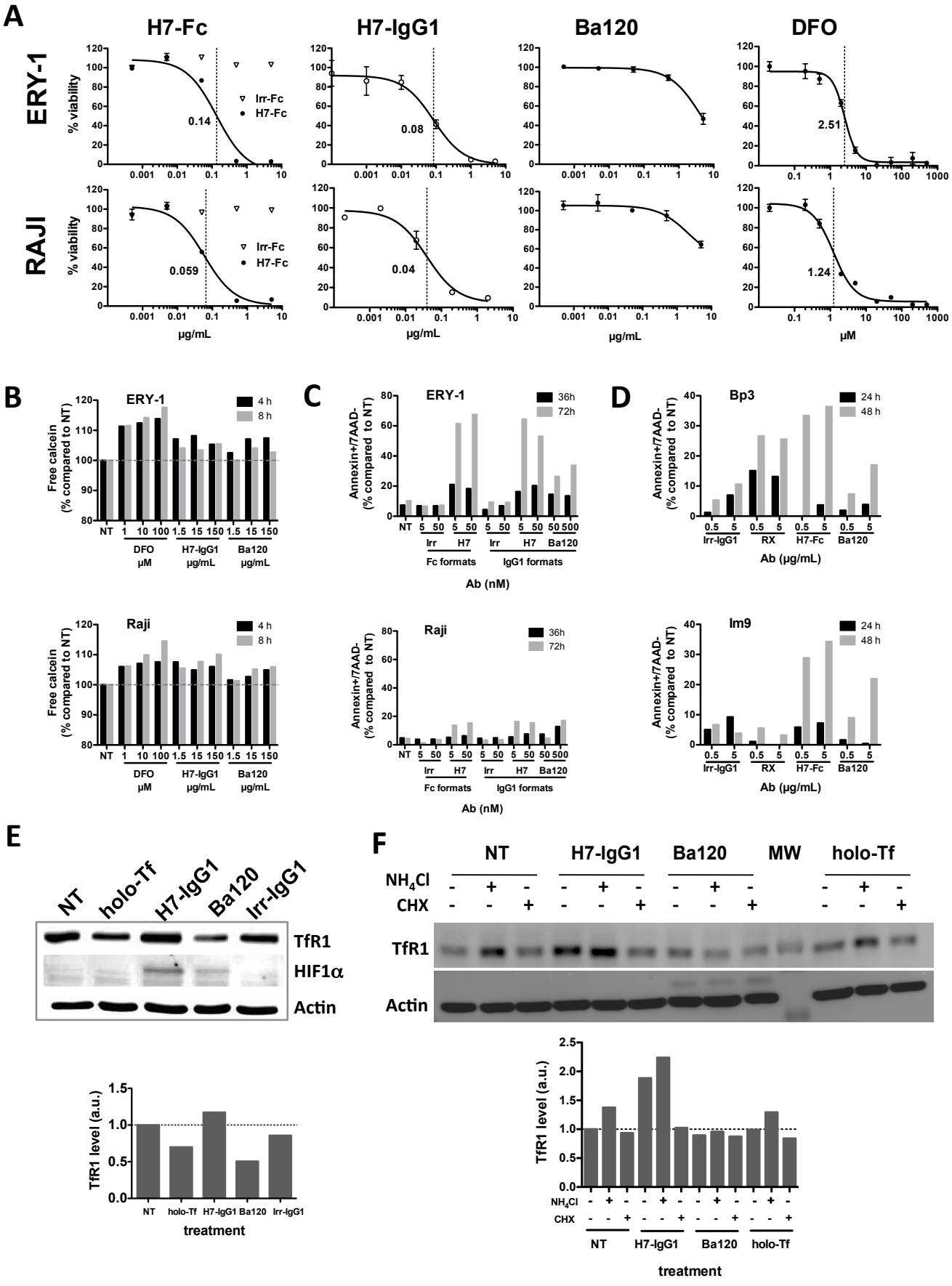
A
H7-Fc
H7-IgG1
Ba120
DFO
ERY-1
RAJI
% viability
Irr-Fc
H7-Fc
0.14
0.08
2.51
0.059
0.04
1.24
µg/mL
µM
B
ERY-1
Raji
4 h
8 h
Free calcein (% compared to NT)
NT
DFO µM
H7-IgG1 µg/mL
Ba120 µg/mL
C
ERY-1
Raji
36h
72h
Annexin+/7AAD- (% compared to NT)
Irr
H7
Fc formats
IgG1 formats
Ab (nM)
D
Bp3
Im9
24 h
48 h
Irr-IgG1
RX
H7-Fc
Ba120
Ab (µg/mL)
E
NT
holo-Tf
H7-IgG1
Ba120
Irr-IgG1
TfR1
HIF1α
Actin
TfR1 level (a.u.)
treatment
F
NT
H7-IgG1
Ba120
MW
holo-Tf
NH4Cl
CHX
TfR1
Actin
TfR1 level (a.u.)
treatment

Figure 4

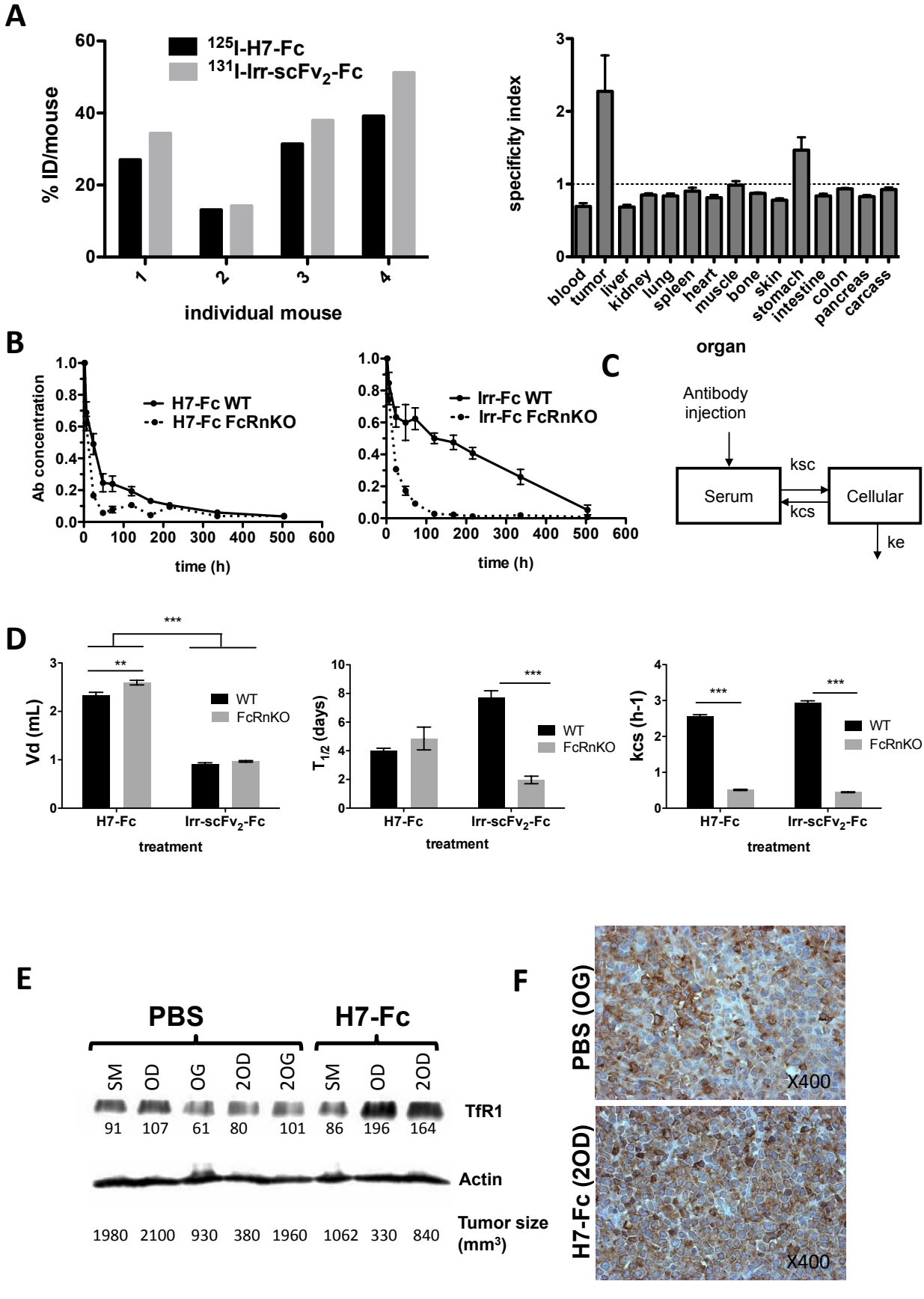
A
125I-H7-Fc
131I-Irr-scFv2-Fc
% ID/mouse
individual mouse
specificity index
blood
tumor
liver
kidney
lung
spleen
heart
muscle
bone
skin
stomach
intestine
colon
pancreas
carcass
organ
B
Ab concentration
H7-Fc WT
H7-Fc FcRnKO
time (h)
Irr-Fc WT
Irr-Fc FcRnKO
time (h)
C
Antibody injection
Serum
Cellular
ksc
kcs
ke
D
Vd (mL)
WT
FcRnKO
H7-Fc
Irr-scFv2-Fc
treatment
T1/2 (days)
kcs (h-1)
E
PBS
H7-Fc
SM
OD
OG
2OD
2OG
TfR1
91 107 61 80 101 86 196 164
Actin
Tumor size (mm3)
1980 2100 930 380 1960 1062 330 840
F
PBS (OG)
H7-Fc (2OD)
X400

Figure 5

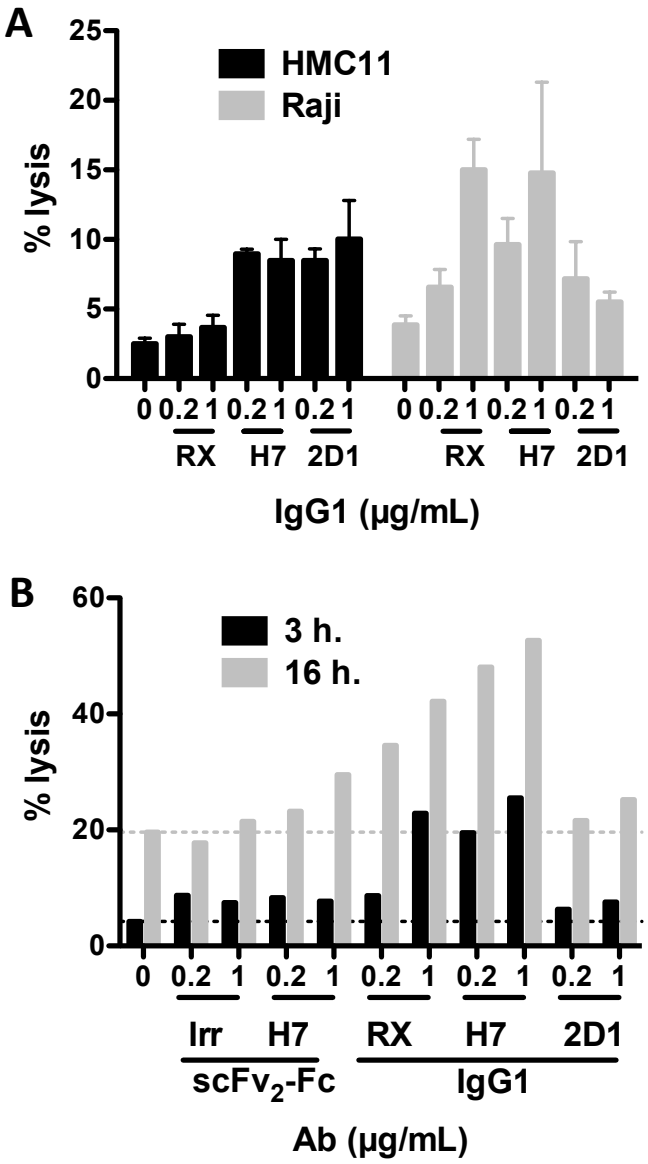
A
25
20
15
10
5
0
% lysis
HMC11
Raji
0 0.2 1 0.2 1 0.2 1 0 0.2 1 0.2 1 0.2 1
RX H7 2D1 RX H7 2D1
IgG1 (µg/mL)
B
60
40
20
0
% lysis
3 h.
16 h.
0 0.2 1 0.2 1 0.2 1 0.2 1 0.2 1
Irr H7 RX H7 2D1
scFv2-Fc IgG1
Ab (µg/mL)

Figure 6

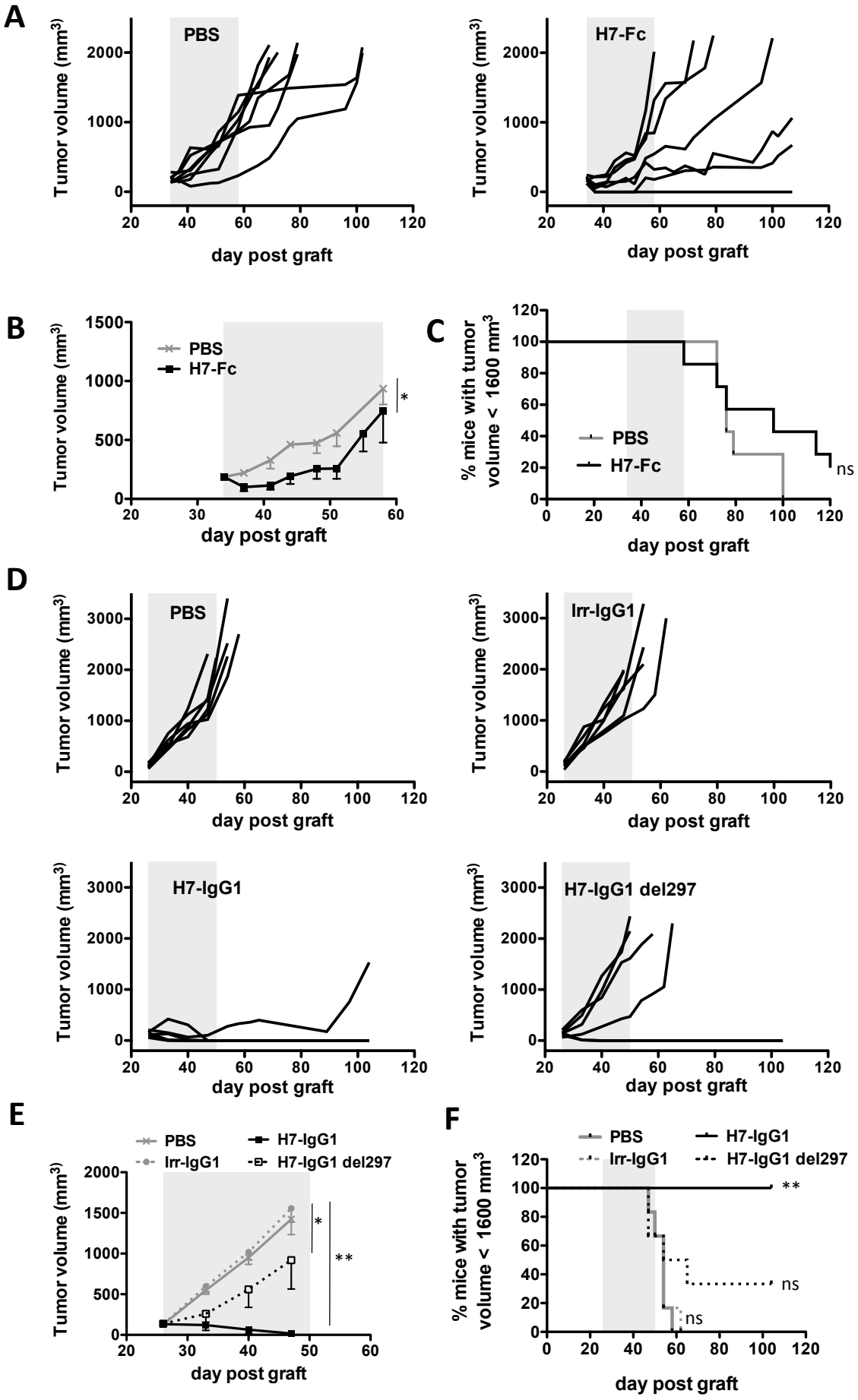
A
PBS
H7-Fc
Tumor volume (mm3)
day post graft
B
PBS
H7-Fc
*
C
% mice with tumor volume < 1600 mm3
ns
D
PBS
Irr-IgG1
H7-IgG1
H7-IgG1 del297
E
F
**
ns

Supplementary material

Material and methods

scFv$_2$-Fc and full length IgG1 antibody design and production

To obtain scFv fused with the Fc fragment of human IgG1, the cDNA encoding the six anti-TfR1 scFv antibodies[1] or anti-botulinum toxin (negative control)[1] were *Nco*I/*Not*I-digested from the phagemid pHEN[2] and subcloned into the pFUSE-hFc2(IL2ss) vector[3], a gift from Frank Perez, CNRS-Institut Curie, Paris, France. Soluble 100 kD scFv$_2$-Fc antibodies were produced after transient transfection of HEK-293 T cells and purified using protein A affinity chromatography, as previously described in Ref.[4]. Full length H7-IgG1 (CK isotype for the light chain) and 2D1-IgG1 (anti-CD117 antibody)[4] were produced in CHO cells from their VH and VL sequences by EVITRIA (EVITRIA, Switzerland). C32-IgG1, F2-IgG1, H9-IgG1, G9-IgG1, H7-IgG1 del297 (that has reduced affinity for Fcγ receptors and C1q due to deletion of the Asn297 residue)[5] and the anti-TfR1 mouse mAb Ba120[6] were a gift from Alexandre Fontayne (LFB, France). The apparent affinities for TfR1 of the two H7-IgG1 and H7-IgG1 del297 were identical (not shown). Rituximab was from Roche. The irrelevant IgG1 antibody was a human polyclonal IgG (SIGMA, I2511). Antibody concentrations were verified by measuring their A_{280nm} by spectrophotometry (1 UA at 280 nm corresponds to 0.8 mg/mL) and purity was checked by SDS-PAGE.

Cell lines

The B-cell lymphoma Bp3, Im9[7] (a gift from Nathalie Bonnefoy, IRCM) and Raji B-cell lymphoma cell lines, the erythroleukemia ERY-1 cell line (a gift from Michel Arock, LBPA, ENS Cachan, France),[8] and the BxPC3 and CFPAC pancreatic cancer cell lines

(obtained from ATCC) were grown in RPMI-Glutamax supplemented with 10% fetal bovine serum (FBS; ThermoScientific SV30160.03) and with penicillin/streptomycin (Gibco 15240-062). The mouse P815 (a gift from Nicolas Fazilleau, Institut Pasteur, Paris, France) and human HMC11 mastocytoma (a gift from Michel Arock, ENS Cachan, France) cell lines were grown in IMDM. Adherent human embryonic kidney HEK-293 T cells (a gift from Laurent Le Cam, IRCM) were grown in DMEM, 10% FBS and antibiotics. All cell lines were cultured at 37°C in a humidified atmosphere with 5% CO_2 and screened monthly for mycoplasma infection.

Commercial antibodies and reagents for FACS, western blotting and IHC

Anti-human CD71 (Invitrogen, 136800), -HIF1-α (Santa Cruz Biotechnology, sc-8711), and -beta-actin (Cell Signaling Technology 3700S) antibodies were used for western blotting. PE-conjugated anti-mouse TfR1 (BD Pharmingen, 553267), APC-conjugated anti-human TfR1 (BD Pharmingen 551374), FITC-conjugated goat anti-human Fc (SIGMA, F9512) or anti-mouse Fc (Invitrogen, 31569) antibodies were used for FACS analysis of TfR1 levels. Anti-human TfR1 (SIGMA, HPA028598) was used for IHC. Human holo-Tf was from SIGMA (T0665), DFO from Santa Cruz (Sc-203331; stock solution: 50mM in H_20, stored at 4°C), holo-Tf conjugated to Alexa Fluor 488 (holo-Tf-A488) from Invitrogen (T13342; 50 µM solution in PBS stored at 4°C), and calcein-AM from Invitrogen (C3100MP; stock solution: 50 µM in DMSO at -20°C).

Holo-Tf uptake measurement

Raji cells (5×10^5) were washed and resuspended in RPMI medium supplemented with 1% fetal calf serum (FCS) and 500 nM holo-Tf-A488 together or not with antibodies or non-conjugated holo-Tf at 37°C for 3h. Cells were then washed with cold PBS and the

cell fluorescence associated with holo-Tf-A488 uptake measured by FACS (FC500 or Gallios cytometer, Beckman Coulter). Preliminary experiments with an additional incubation of cells with 50mM glycine pH 2.8/500mM NaCl buffer for 10 min at 4°C before FACS analysis showed that the fluorescence measured was more than 95% intracellular. Therefore, this step was omitted in further experiments to limit the steps before analysis (**Figure S1B**). The cell mean fluorescence intensity (MFI) was calculated using the Flow Jo Version 10.1r7 software.

Antibody apparent affinity and antibody/ligand competition

All incubation steps were done on ice. Raji or P815 cells (5×10^5 cells) were resuspended in 100 µL of FACS buffer [PBS, 1% FBS] containing various concentrations of the primary antibody for 1h, washed twice with FACS buffer, and then incubated with the suitable fluorescent secondary antibody. After a final wash, cells were analyzed by FACS. The apparent affinity was determined using the GraphPad software. For competition experiments, cells were incubated with 1nM antibody mixed with increasing concentrations of holo-Tf (0.5pM to 5µM). Then, bound antibodies were detected as before. Alternatively, cells were incubated with 500 nM holo-Tf-A488 mixed with increasing concentrations of antibody (5nM to 500 nM), or with holo-Tf (0.1 nM to 10 µM).

Biacore analysis

SPR analyses were performed on a BIA3000 apparatus at 25°C in HBS-P (GE Healthcare). For affinity measurements, anti-human IgG(Fc) (Human-antibody capture Kit (GE-Healthcare, BR-1008-39) was covalently immobilized on CM5 sensor chip using EDC/NHS activation according to the manufacturer's instructions (GE Healthcare).

Recombinant homodimeric human TfR1 (produced in baculovirus/insect cell expression system from pACGP67A-human TfR1 vector (clone 12130, Addgene))[9] at various concentrations was injected on H7-IgG1 or H7-Fc captured on immobilized anti-human-Fc IgG during 180s. After 400s of dissociation with running buffer, the sensor chip was regenerated using MgCl2 3M. The K_D values, taking into account of affinity and avidity with this protocol, were calculated using a steady-state fitting model (BiaEvaluation3.2, GE Healthcare). For competition analysis, human TfR1 was injected at 20nM during 180s at 50µl/min on H7–IgG1 or H7-Fc captured at a level around 1800 RU. During the dissociation step (very slow dissociation rate), human holo-Tf was injected at different concentrations (1.25-1250nM) to displace human TfR1.

Cell viability assay

Cells (5×10^3) were plated in sixplicates in 96-well U-bottom plates. Antibody solutions diluted in culture medium were added to each well (total volume 200 µL). A well containing only 200 µL of culture medium was also prepared (reference). After 4 to 5 days, cell viability was estimated using the CellTiter 96 AQueous cell proliferation MTS assay (Promega, G5430). Briefly, 20 µL of MTS reagent was added to each well and left for about 2 hours. Plates were then centrifuged and 100 µL of supernatant from each well was transferred to a well of a 96-well plate (flat bottom) for OD reading at 490 nm using a microplate reader (Multiskan).

Apoptosis assay

ERY-1 cells or Raji cells or the B-cell lymphoma Im9 and Bp3 cells (2.5 10^5 cells or 1.5 10^5 cells according to the incubation time) were plated in 6-wells plates in 2ml medium and incubated with various concentrations of antibodies for 24h to 72h. Cells were

collected, stained using the Beckman Coulter IM3614 Apoptosis Kit, as recommended by the manufacturer, and analyzed by FACS. Granularity over size was plotted and small debris excluded for the relative quantification (%) of Annexin-positive and 7-AAD-negative cells that represent early apoptotic cells.

Intracellular free iron detection

Intracellular free iron levels were measured using the fluorescent probe calcein, as previously described Ref.[10]. This probe binds to iron stoichiometrically in a reversible manner, forming fluorescence-quenched calcein-iron complexes. Therefore, higher cell fluorescence means that the levels of intracellular labile iron pool are reduced. Briefly, cells were washed and resuspended in medium without FCS and stained with 250 nM calcein-AM at 37°C for 5min. They were washed with complete medium and resuspended in pre-warmed culture medium with 1% FCS and incubated with the studied antibodies or deferoxamine (DFO) for 4 or 8h. Cell fluorescence due to free calcein was measured by flow cytometry and the percentage increase in calcein fluorescence relative to untreated control was calculated.

Western blotting

Raji cells (5.10^5 cells in 2 mL) were treated as indicated in the figure legends for 18 h or 36 h. Cells were harvested, centrifuged and washed with cold PBS. Proteins were extracted with 100 µL of boiling lysis buffer (1% SDS, 1 mM sodium orthovanadate, 10 mM Tris pH 7.4)/cell pellet. The viscous mix was sonicated on ice four times at 25mA for 5s, and then centrifuged. Protein concentration was determined using the BCA assay (Interchim). Proteins were extracted from tumor samples using a lysis buffer containing 1% Triton-X100, 0.5% NP40, 1 mM EDTA, 150 mM NaCl, 10 mM Tris-Hcl pH 7.5, 100

mM NaF, 1 mM sodium orthovanadate, 2 mM phenylmethylsulfonyl fluoride complemented with 1 tablet of protease inhibitors mixture for 10 mL (Roche Diagnostics). A piece of tumor of 10 mm^3 was cut into small pieces, and then 0.5 mL of lysis buffer was added at 4°C for 30min, followed by grinding with glass beads using a Retsch MM300 TissueLyser (Qiagen) at maximum power for 3 min, followed by incubation at 4°C for 30 min. Protein extracts were centrifuged (12,000g at 4°C for 30 min), and proteins in the soluble fraction quantified with the BCA assay. For western blotting, 20 µg of protein were separated by SDS-PAGE on 7% polyacrylamide separation gels and transferred to PVDF membranes. Membranes were blocked with PBS/0.1% Tween-5% milk at room temperature (RT) for 2h. Incubations with primary and secondary antibodies were done overnight at 4°C and 1h at RT, respectively. Membranes were revealed with Western Lightning PLUS-ECL (Perkin Elmer) and analyzed with a G-box (Syngene). Quantification was done using the ImageJ software.

ADCC

Raji or HMC11 cells were stained with the PKH26 Red Fluorescent Cell Linker Mini Kit (SIGMA, Mini26-1 KT) following the manufacturer's instructions. Briefly, cells were harvested and stained with PKH26 fluorescent dye at RT for 3 min, washed and then cultured in complete medium overnight. Stained cells (50,000 cells; 50 µL/well) were then transferred in 96-well U-bottom plates and combined with 50 µL of rituximab (anti-CD20), 2D1 (anti-CD117), H7-IgG1 or H7-Fc (0.2 or 1 µg/mL final) at 37°C for 30min. Peripheral Blood Mononuclear cells (PBMC) (50 µL, 2.5 10^6 cells) isolated from normal human blood using Ficoll were added to the mixture (effector to target cell ratio of 50). After 3h of incubation at 37°C, cells were collected and stained with 7-AAD (0.1

µg/mL final) at 4°C for 15min before FACS analysis. The percentage of 7-AAD$^+$ cells among the PKH26$^+$ cells represented the target cells killed by PBMC.

Determination of scFv$_2$-Fc concentration in serum samples by ELISA

Blood samples were centrifuged at 1500g for 15 min, and serum samples were stored at -20°C until dilution (1000 times in PBS) and scFv$_2$-Fc titration by ELISA. An ELISA sandwich assay (linear range from 10 to 150 ng /mL) was specifically developed using a goat anti-human Fc as the capture antibody (Sigma, I-2126, 10 µg/mL) and a HRP-conjugated goat anti-human-Fc antibody as the detection antibody (A0170, dilution 20 000). Samples were tested in duplicate and tittered in two independent ELISA experiments.

In vivo experiments

All *in vivo* experiments were performed in compliance with the French regulations and ethical guidelines for experimental animal studies in an accredited establishment. In some experiments, tumors were isolated and prepared for IHC analysis with an anti-TfR1 antibody (IRCM Histology core facility) or for protein extraction for western blotting.

Statistical analysis (in vivo study for therapeutic efficiency)

A linear mixed regression model was used to determine the relationship between tumor growth and the number of days post-graft. The fixed part of the model included variables corresponding to the number of days post-graft and the different groups. Interaction terms were built into the model. Random intercept and random slope were included to take into account the time effect. The coefficients of the model were

estimated by maximum likelihood and considered significant at the 0.05 level. Survival rates were estimated using the Kaplan-Meier method from the date of the xenograft until the date when the tumor reached a volume of 1,600 mm^3. Survival curves were compared using the log-rank test. Statistical analyses were carried out using the STATA 11.0 software (StataCorp, College Station, TX).

References

1. Goenaga AL, Zhou Y, Legay C, Bougherara H, Huang L, Liu B, et al. Identification and characterization of tumor antigens by using antibody phage display and intrabody strategies. Molecular immunology 2007; 44:3777-88.

2. Hoogenboom HR, Griffiths AD, Johnson KS, Chiswell DJ, Hudson P, Winter G. Multi-subunit proteins on the surface of filamentous phage: methodologies for displaying antibody (Fab) heavy and light chains. Nucleic Acids Res 1991; 19:4133-7.

3. Moutel S, El Marjou A, Vielemeyer O, Nizak C, Benaroch P, Dubel S, et al. A multi-Fc-species system for recombinant antibody production. BMC Biotechnol 2009; 9:14.

4. Le Gall M, Crepin R, Neiveyans M, Auclair C, Fan Y, Zhou Y, et al. Neutralization of KIT Oncogenic Signaling in Leukemia with Antibodies Targeting KIT Membrane Proximal Domain 5. Molecular cancer therapeutics 2015; 14:2595-605.

5. Tao MH, Morrison SL. Studies of aglycosylated chimeric mouse-human IgG. Role of carbohydrate in the structure and effector functions mediated by the human IgG constant region. J Immunol 1989; 143:2595-601.

6. Loisel S, Andre PA, Golay J, Buchegger F, Kadouche J, Cerutti M, et al. Antitumour effects of single or combined monoclonal antibodies directed against membrane antigens expressed by human B cells leukaemia. Molecular cancer 2011; 10:42.

7. Brien G, Trescol-Biemont MC, Bonnefoy-Berard N. Downregulation of Bfl-1 protein expression sensitizes malignant B cells to apoptosis. Oncogene 2007; 26:5828-32.

8. Ribadeau Dumas A, Hamouda NB, Leriche L, Piffaut MC, Bonnemye P, Kuen RL, et al. Establishment and characterization of a new human erythroleukemic cell line, ERY-1. Leuk Res 2004; 28:1329-39.

9. Lebron JA, Bennett MJ, Vaughn DE, Chirino AJ, Snow PM, Mintier GA, et al. Crystal structure of the hemochromatosis protein HFE and characterization of its interaction with transferrin receptor. Cell 1998; 93:111-23.

10. Roth M, Will B, Simkin G, Narayanagari S, Barreyro L, Bartholdy B, et al. Eltrombopag inhibits the proliferation of leukemia cells via reduction of intracellular iron and induction of differentiation. Blood 2012; 120:386-94.

11. Bourquard T, Musnier A, Puard V, Tahir S, Ayoub MA, Jullian Y, et al. MAbTope: A Method for Improved Epitope Mapping. J Immunol 2018; 201:3096-105.

12. Lawrence CM, Ray S, Babyonyshev M, Galluser R, Borhani DW, Harrison SC. Crystal structure of the ectodomain of human transferrin receptor. Science 1999; 286:779-82.

13. Webb B, Sali A. Comparative Protein Structure Modeling Using MODELLER. Current Protocols in Bioinformatics: John Wiley & Sons, Inc., 2014:5.6.1-5.6.32.

14. Dang S, MacColl R, Parsons P. Spectroscopic study of the interaction of aluminum ions with human transferrin. J Inorg Biochem 1995; 60:175-85.

Table S1 : $scFv_2$-Fc antibody formats classic pharmacokinetic constants

mouse phenotype	mAb	AUC ($mg.h.mL^{-1}$)	CL ($mL.h^{-1}$)
WT	H7-Fc	4.0 [3.3-5.2]	0.98 [0.93-1.02]
	Irr-Fc	16,1 [13.0–18.6]	0.40 [0.36-0.43]
FcRn KO	H7-Fc	2.4 [1.3–4.0]	3.30 [3.13-3.38]
	Irr-Fc	3.3 [2.5–4.4]	1.31 [1.27-1.35]

AUC*, Area Under the Curve calculated from day 0 to day 21, CL, serum clearance; numbers in brackets represent maxima and minima within the groups of 10 mice. Irr-Fc, irrelevant $scFv_2$-Fc.*

In the WT background, H7-Fc binding to mouse TfR1 decreases the AUC and increase CL compared to the non specific counterpart format. AUC of the irrelevant $scFv_2$-Fc drastically decreases and its CL increases in the FcRnKO background because the antibody is not protected by the FcRn.
The results obtained for the H7-Fc, where the AUC slightly decreases and the CL strongly increases in the FcRnKO background, could indicate that, since FcRn and TfR1 colocalize in the recycling intracellular trafficking pathway, the binding of H7-Fc to TfR1 is enhanced in the absence of FcRn through limitation of steric hindrance that occurs I case of double binding. This remains to be confirmed by further investigations.

Supplementary figure legends:

Figure S1: Setting up of the holo-Tf cell internalization test

(**A, B**) Raji cells were incubated at 37°C or 4°C (to allow or not internalization, respectively) with 500 nM holo-Tf conjugated to Alexa-488 (holo-Tf-A488) in culture medium for the indicated times. Cells were then washed with PBS, incubated or not with NaCl-glycine buffer (50 mM glycine pH 2.8, 500 mM NaCl) at 4°C for 10min, then washed again with PBS to remove surface-bound holo-Tf-A488, and cell fluorescence was measured by FACS. Total, fluorescence in cells without glycine step; intracellular, fluorescence in cells with glycine step. Fluorescence increased from 1 to 3h and was more than 95% intracellular; therefore, the glycine incubation step was omitted in further experiments. The cell mean fluorescence intensity (MFI) was calculated using the Flow Jo Version 10.1r7 software. (**C**) Raji cells were incubated with 500 nM holo-Tf-

A488 together with increasing concentrations of unconjugated holo-Tf at 37°C for 3h. Increasing concentrations of unconjugated holo-Tf reduced fluorescence accumulation (IC_{50} = 580 nM) in a dose-dependent manner, showing the specificity of the holo-Tf internalization test.

Figure S2: SPR analysis of H7-Fc and H7-IgG1 interactions with recombinant human TfR1 and competition with holo-Tf

(**A,B**) Various concentrations (0.25-32 nM) of homodimeric human recombinant TfR1 were injected on H7-Fc or H7-IgG1 captured on immobilized anti-human-Fc IgG. The KD values, taking into account of affinity and avidity with this protocol, were calculated using a steady-state fitting model. H7-Fc and H7-IgG1 display similar KD (5 nM). (**C**) Human TfR1 was injected on H7-Fc or H7-IgG1 immobilized onto anti-human-Fc IgG. Human holo-Tf was injected at the indicated concentrations to displace human TfR1. Higher concentrations of holo-Tf were required to quantitatively release human TfR1 from H7-Fc than from H7-IgG1, consistent with the results obtained in the competition experiment for holo-Tf internalization on cells of figure 1D where H7-Fc blocks holo-Tf internalization better than H7-IgG1.

Figure S3: 3D modeling of the interaction of H7 and Ba120 with human TfR1

(A) Modeling of the interaction of H7 (red) and Ba120 (green) with human TfR1 (grey) using their VH and VL amino acid sequences. Docking of both antibodies on human TfR1 was done with MabTope,[11] using 3D models of the antibodies and the 3D structure of the ectodomain of human TfR1 (PDB:1CX8).[12] The 3D models of both antibodies were made using Modeller[13] and the templates PDB:3F12 for H7 VH, PDB:3MA9 for H7 VL, 3BZH for

Ba120 VH and 3L7E for Ba120 VL (NB: Ba120 sequences were determined from the original hybridoma by Dr. Martine Cerutti, CNRS, Saint Christol-Les-Ales, France). **(B),** Representation of the interaction of human holo-Tf (blue, from PDB 1SUV) with human TfR1. This model predicts that H7 competes directly with holo-Tf binding, while Ba120 and holo-Tf can bind to TfR1 at the same time, in agreement with the in vitro experimental data (**Figure 2**). Figures were prepared using Pymol (The PyMOL Molecular Graphics System, Version 2.0 Schrödinger, LLC). MAbTope is a coarse-grained protein-protein docking method, it doesn't use force fields, neither energy minimization and there's no solvent. MAbTope uses HEX for docking poses generation. HEX generates about 10^8 poses. The top-500 HEX poses are then reranked using different scoring functions, of which one is learnt on two datasets of protein-protein complexes of known structures. We have shown that on a benchmark of 129 antibody-antigen complexes the top-30 ranked conformations correctly define the epitope, and that in 80% cases, one near-native docking pose is present in the top-30. For the figure, one docking pose for each antibody has been manually chosen within the top-30. Thus, there is no guaranty that the orientation of the antibody relative to the target is correct, however the pose correctly defines the epitope on the TfR1.

Figure S4: Variation of intracellular iron levels in the Bp3 and the Im9 B-lymphoma cell lines upon H7 treatment.

The same protocol than **Figure 3B** was applied. Results are expressed as the % of change in the fluorescence relative to non treated cells (NT). In Bp3 and Im9 cell lines, H7 induced only low soluble iron decrease compared to ERY or Raji cell lines (see Figure

3B) and Ba120 induced an increase in soluble iron levels, in agreement with its ability to accelerate holo-Tf uptake mediated by TfR1 (**see figure 2A, left panel**).

Figure S5: Comparison of H7-IgG1, Ba120 and human-holo-Tf binding to native human TfR1 at different pH values

The protocol described in **(A)** was used to study H7-IgG1 binding to TfR1 at different pH values, similar to those encountered during physiological TfR1 internalization and recycling after holo-Tf binding. The experiment was performed at 4°C. Raji cells were incubated with anti-TfR1 antibodies (10 µg/mL) or human holo-Tf conjugated to Alexa488 (500 nM) at pH 7 for 1h. Unbound antibodies or holo-Tf were eliminated by washing at pH 7, and then cells were incubated at a given pH (from 7 to 5), to mimic the conditions within endosomes after internalization (1 h at 4°C). A final wash was performed at pH 7, to mimic the conditions after TfR1 recycling at the cell surface. FITC-conjugated anti-human or mouse IgG secondary antibodies were used to detect by FACS the remaining bound antibodies after these steps. **(B)** Results are expressed as the percentage of the Mean Fluorescent Intensity (MFI) relative to the MFI of cells kept at pH 7 for the entire experiment. As expected, holo-Tf binding decreased at lower pH, because of the loss of Fe^{3+} at low pH and the reduced affinity of apo-Tf at pH 7. **(C)** The iron content of holo-Tf at various pH values was monitored by taking advantage of the fact that holo-Tf, but not apo-Tf, displays an absorption peak at 460 nm.[14] Holo-Tf (10 µM) was resuspended in buffer at various pH. Results are expressed as the ratio of the sample absorbance at 460 nm normalized to the standard protein concentration obtained at 280 nm.

Figure S6. Biodistribution of the cross-reactive anti-TfR1 H7 scFv$_2$-Fc (H7-Fc) antibody in mice with tumors

The four nude mice bearing ERY-1 tumors that received one *i.v.* injection of a mixture of ^{125}I-labeled H7-Fc and ^{131}I-labeled irrelevant scFv$_2$-Fc used in **Figure 4** were killed at 48h post-injection, and the radioactivity in all organs and tissues was quantified as in **Figure 4**. Results are expressed as the % of the injected dose (ID) per g (%ID/g). H7-Fc accumulated in the tumor.

Figure S7. ADCC on BxPC3 and CFPAC cells using the anti-TfR1 H7 scFv$_2$-Fc and full length IgG1 antibodies

ADCC was evaluated in live BxPC3 or CFPAC cells (both derived from a pancreatic ductal adenocarcinoma) with the same protocol used for Raji cells in **Figure 5.** Briefly, cells were stained with the fluorescent dye PKH-67, and the day after were incubated with H7-Fc or H7-IgG1, or an irrelevant scFv$_2$-Fc antibody (0.2 or 1 µg/mL final concentration) for 30min. Then, freshly prepared PBMC (Effector/Target ratio = 50) were added for 3h. Cells were then collected and stained with the 7-AAD fluorescent dye. The percentage of dead cells (7AAD$^+$) cells among the target PKH-67$^+$ cells was evaluated by FACS analysis. The H7-IgG1 antibody was more efficient than H7-Fc to mediate ADCC of BxPC3 and CFPAC cells, as already observed in Raji cells (**Figure 5**).

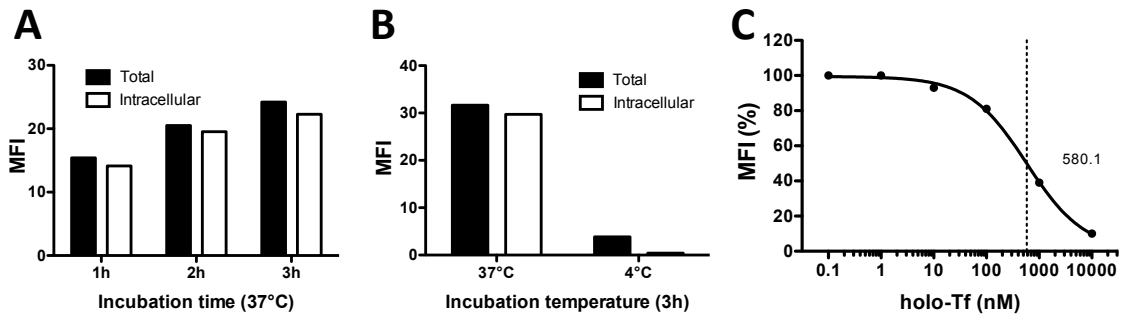

Figure S1: Setting up of the holo-Tf cell internalization test

(**A, B**) Raji cells were incubated at 37°C or 4°C (to allow or not internalization, respectively) with 500 nM holo-Tf conjugated to Alexa-488 (holo-Tf-A488) in culture medium for the indicated times. Cells were then washed with PBS, incubated or not with NaCl-glycine buffer (50 mM glycine pH 2.8, 500 mM NaCl) at 4°C for 10min, then washed again with PBS to remove surface-bound holo-Tf-A488, and cell fluorescence was measured by FACS. Total, fluorescence in cells without glycine step; intracellular, fluorescence in cells with glycine step. Fluorescence increased from 1 to 3h and was more than 95% intracellular; therefore, the glycine incubation step was omitted in further experiments. The cell mean fluorescence intensity (MFI) was calculated using the Flow Jo Version 10.1r7 software. (**C**) Raji cells were incubated with 500 nM holo-Tf-A488 together with increasing concentrations of unconjugated holo-Tf at 37°C for 3h. Increasing concentrations of unconjugated holo-Tf reduced fluorescence accumulation (IC_{50} = 580 nM) in a dose-dependent manner, showing the specificity of the holo-Tf internalization test.

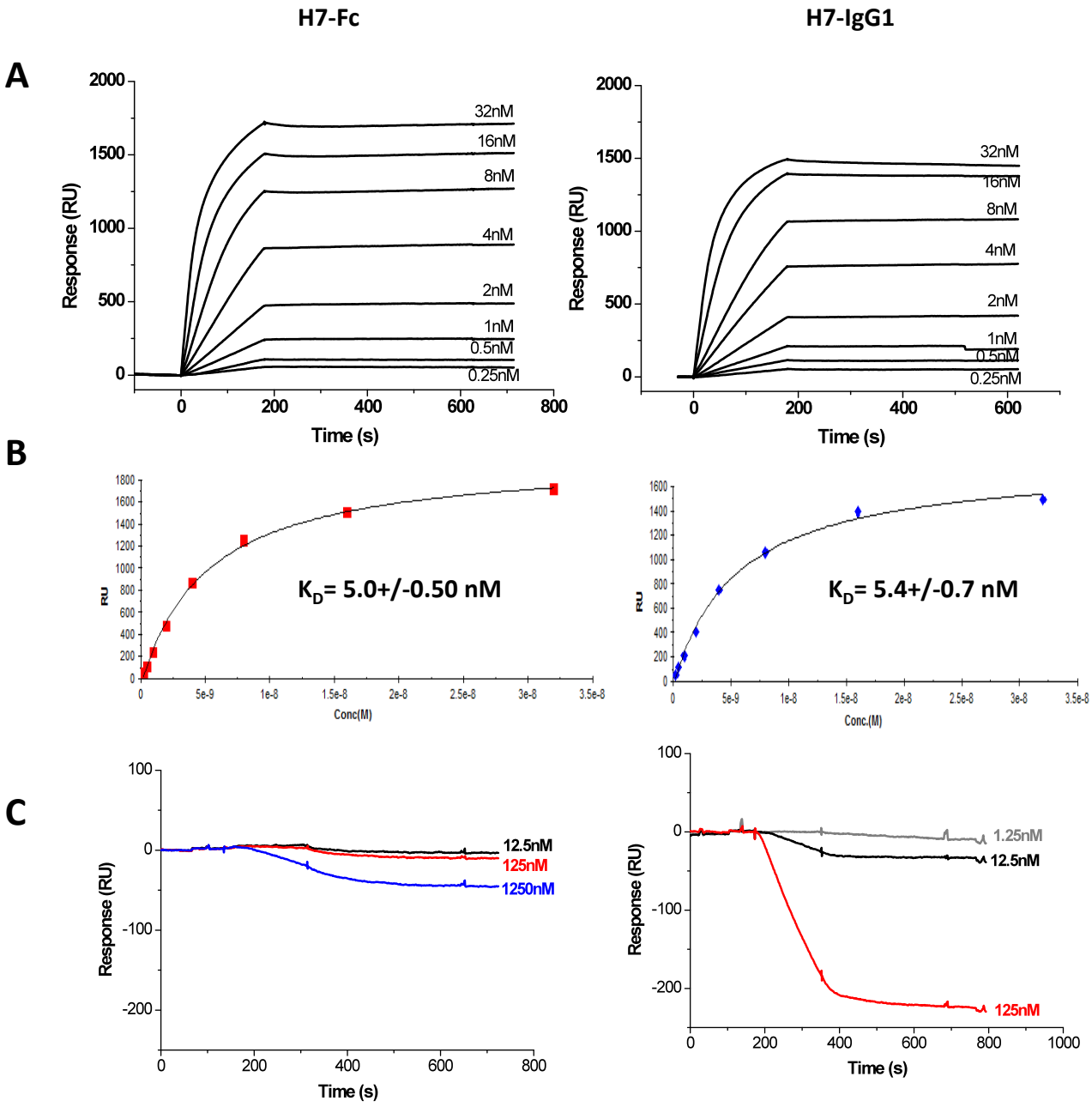

Figure S2: SPR analysis of H7-Fc and H7-IgG1 interactions with recombinant human TfR1 and competition with holo-Tf

(**A,B**) Various concentrations (0.25-32 nM) of homodimeric human recombinant TfR1 were injected on H7-Fc or H7-IgG1 captured on immobilized anti-human-Fc IgG. The KD values, taking into account of affinity and avidity with this protocol, were calculated using a steady-state fitting model. H7-Fc and H7-IgG1 display similar KD (5 nM). (**C**) Human TfR1 was injected on H7-Fc or H7-IgG1 immobilized onto anti-human-Fc IgG. Human holo-Tf was injected at the indicated concentrations to displace human TfR1. Higher concentrations of holo-Tf were required to quantitatively release human TfR1 from H7-Fc than from H7-IgG1, consistent with the results obtained in the competition experiment for holo-Tf internalization on cells of figure 1D where H7-Fc blocks holo-Tf internalization better than H7-IgG1.

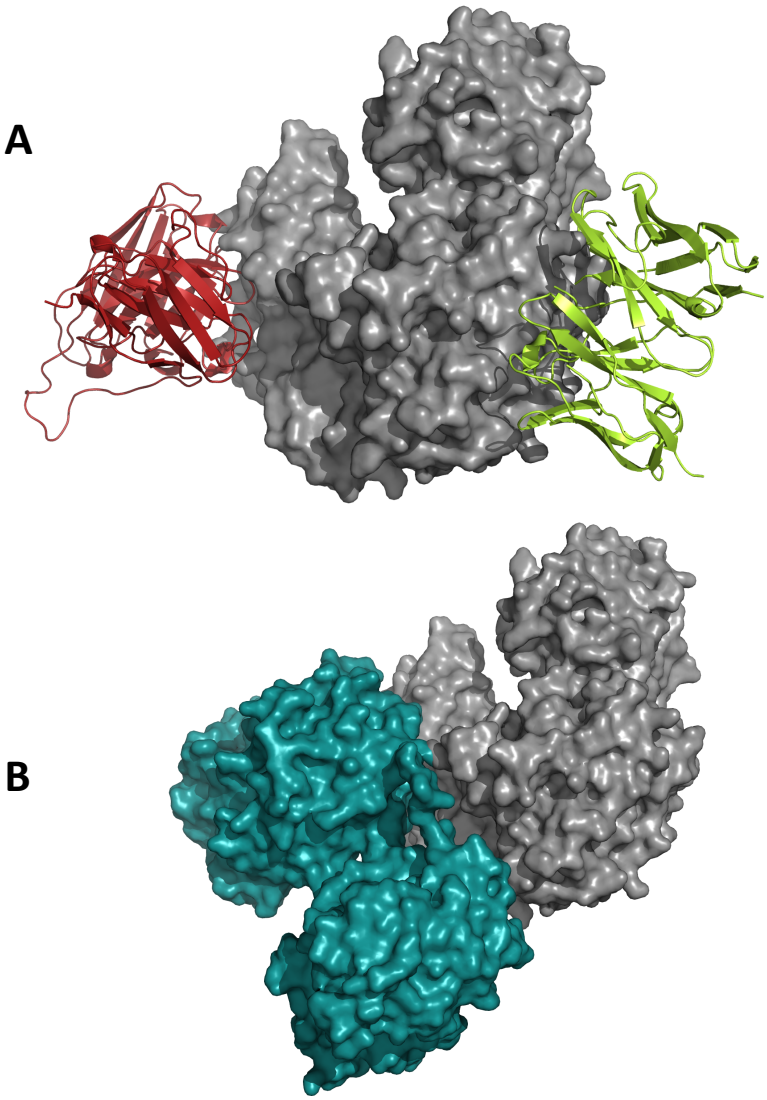

Figure S3: 3D modeling of the interaction of H7 and Ba120 with human TfR1
(A) Modeling of the interaction of H7 (red) and Ba120 (green) with human TfR1 (grey) using their VH and VL amino acid sequences. Docking of both antibodies on human TfR1 was done with MabTope,[11] using 3D models of the antibodies and the 3D structure of the ectodomain of human TfR1 (PDB:1CX8).[12] The 3D models of both antibodies were made using Modeller[13] and the templates PDB:3F12 for H7 VH, PDB:3MA9 for H7 VL, 3BZH for Ba120 VH and 3L7E for Ba120 VL (NB: Ba120 sequences were determined from the original hybridoma by Dr. Martine Cerutti, CNRS, Saint Christol-Les-Ales, France). **(B),** Representation of the interaction of human holo-Tf (blue, from PDB 1SUV) with human TfR1. This model predicts that H7 competes directly with holo-Tf binding, while Ba120 and holo-Tf can bind to TfR1 at the same time, in agreement with the in vitro experimental data (**Figure 2**). Figures were prepared using Pymol (The PyMOL Molecular Graphics System, Version 2.0 Schrödinger, LLC). MAbTope is a coarse-grained protein-protein docking method, it doesn't use force fields, neither energy minimization and there's no solvent. MAbTope uses HEX for docking poses generation. HEX generates about 10^8 poses. The top-500 HEX poses are then reranked using different scoring functions, of which one is learnt on two datasets of protein-protein complexes of known structures. We have shown that on a benchmark of 129 antibody-antigen complexes the top-30 ranked conformations correctly define the epitope, and that in 80% cases, one near-native docking pose is present in the top-30. For the figure, one docking pose for each antibody has been manually chosen within the top-30. Thus, there is no guaranty that the orientation of the antibody relative to the target is correct, however the pose correctly defines the epitope on the TfR1.

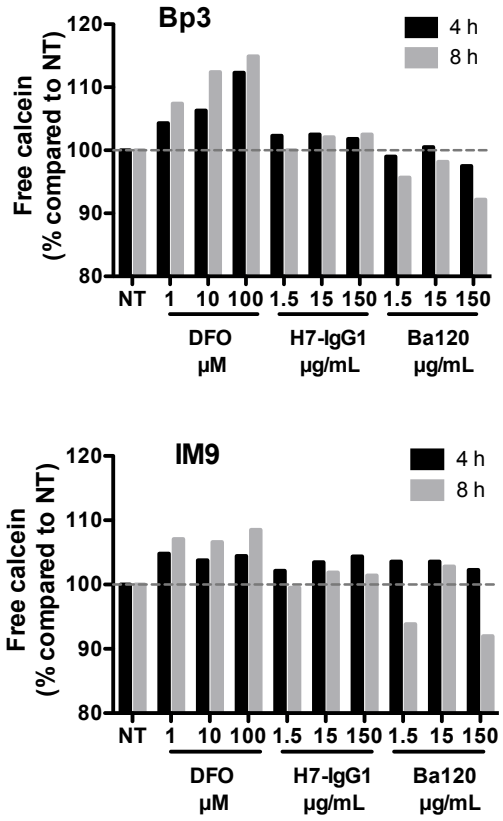

Figure S4: Variation of intracellular soluble iron levels in the Bp3 and the Im9 B-lymphoma cell lines upon H7 treatment.

The same protocol than **Figure 3B** was applied. Results are expressed as the % of change in the fluorescence relative to non treated cells (NT). In Bp3 and Im9 cell lines, H7 induced only low soluble iron decrease compared to ERY or Raji cell lines (see Figure 3B) and Ba120 induced an increase in soluble iron levels, in agreement with its ability to accelerate holo-Tf uptake mediated by TfR1 (**see figure 2A, left panel**).

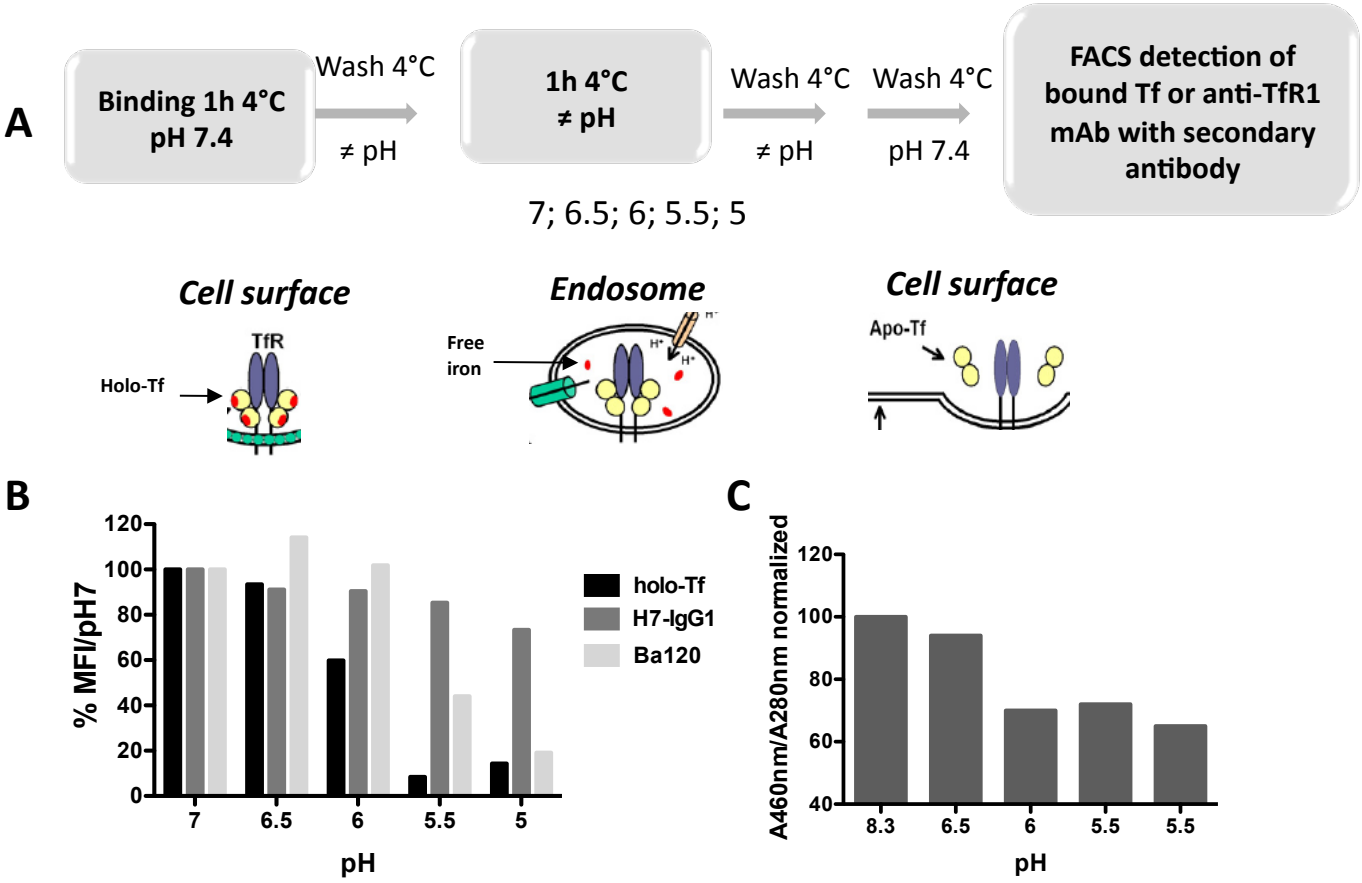

Figure S5: Comparison of H7-IgG1, Ba120 and human-holo-Tf binding to native human TfR1 at different pH values

The protocol described in **(A)** was used to study H7-IgG1 binding to TfR1 at different pH values, similar to those encountered during physiological TfR1 internalization and recycling after holo-Tf binding. The experiment was performed at 4°C. Raji cells were incubated with anti-TfR1 antibodies (10 µg/mL) or human holo-Tf conjugated to Alexa488 (500 nM) at pH 7 for 1h. Unbound antibodies or holo-Tf were eliminated by washing at pH 7, and then cells were incubated at a given pH (from 7 to 5), to mimic the conditions within endosomes after internalization (1 h at 4°C). A final wash was performed at pH 7, to mimic the conditions after TfR1 recycling at the cell surface. FITC-conjugated anti-human or mouse IgG secondary antibodies were used to detect by FACS the remaining bound antibodies after these steps. **(B)** Results are expressed as the percentage of the Mean Fluorescent Intensity (MFI) relative to the MFI of cells kept at pH 7 for the entire experiment. As expected, holo-Tf binding decreased at lower pH, because of the loss of Fe^{3+} at low pH and the reduced affinity of apo-Tf at pH 7. **(C)** The iron content of holo-Tf at various pH values was monitored by taking advantage of the fact that holo-Tf, but not apo-Tf, displays an absorption peak at 460 nm.[14] Holo-Tf (10 µM) was resuspended in buffer at various pH. Results are expressed as the ratio of the sample absorbance at 460 nm normalized to the standard protein concentration obtained at 280 nm.

A

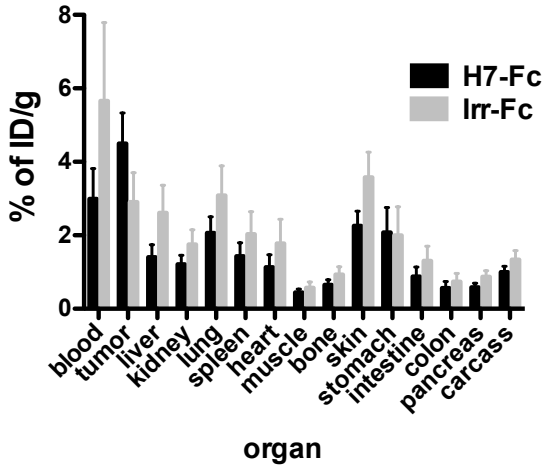

Figure S6. Biodistribution of the cross-reactive anti-TfR1 H7 scFv$_2$-Fc (H7-Fc) antibody in mice with tumors

The four nude mice bearing ERY-1 tumors that received one *i.v.* injection of a mixture of ^{125}I-labeled H7-Fc and ^{131}I-labeled irrelevant scFv$_2$-Fc used in **Figure 4** were killed at 48h post-injection, and the radioactivity in all organs and tissues was quantified as in **Figure 4.** Results are expressed as the % of the injected dose (ID) per g (%ID/g). H7-Fc accumulated in the tumor.

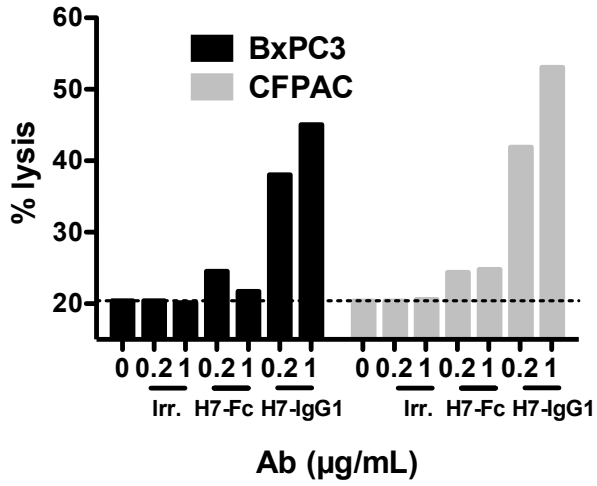

Figure S7. ADCC on BxPC3 and CFPAC cells using the anti-TfR1 H7 scFv2-Fc and full length IgG1 antibodies

ADCC was evaluated in live BxPC3 or CFPAC cells (both derived from a pancreatic ductal adenocarcinoma) with the same protocol used for Raji cells in **Figure 5.** Briefly, cells were stained with the fluorescent dye PKH-67, and the day after were incubated with H7-Fc or H7-IgG1, or an irrelevant $scFv_2$-Fc antibody (0.2 or 1 µg/mL final concentration) for 30min. Then, freshly prepared PBMC (Effector/Target ratio = 50) were added for 3h. Cells were then collected and stained with the 7-AAD fluorescent dye. The percentage of dead cells ($7AAD^+$) cells among the target PKH-67^+ cells was evaluated by FACS analysis. The H7-IgG1 antibody was more efficient than H7-Fc to mediate ADCC on BxPC3 and CFPAC cells by PBMC, as already observed in Raji cells (**Figure 5**).